β decay of ^{127}Cd and excited states in ^{127}In

Ch. Lorenz,[1] L. G. Sarmiento,[1] D. Rudolph,[1] P. Golubev,[1] T. Eronen,[2] D. A. Nesterenko,[2] A. Kankainen,[2] L. Canete,[2] D. M. Cox,[1,2] A. Fernandez,[3] U. Forsberg,[1,2,4] A. Jungclaus,[3] I. Kojouharov,[5] N. Kurz,[5] N. Lalović,[1] J. Partanen,[2] M. Reponen,[2] S. Rinta-Antila,[2] A. de Roubin,[2] A. Såmark-Roth,[1] V. Vaquero,[3] and M. Vilén[2]

[1]*Department of Physics, Lund University, S-22100 Lund, Sweden*
[2]*Department of Physics, University of Jyväskylä, FI-40014 Jyväskylä, Finland*
[3]*Instituto de Estructura de la Materia, CSIC, E-28006 Madrid, Spain*
[4]*Department of Physics, University of York, Heslington, York YO10 5DD, United Kingdom*
[5]*GSI Helmholtzzentrum für Schwerionenforschung, D-64291 Darmstadt, Germany*

(Received 10 December 2018; revised manuscript received 12 February 2019; published 19 April 2019)

A dedicated spectroscopic study of the β decay of ^{127}Cd was conducted at the IGISOL facility at the University of Jyväskylä. Following high-resolution mass separation in a Penning trap, β-γ-γ coincidences were used to considerably extend the decay scheme of ^{127}In. The β-decaying $3/2^+$ and $11/2^-$ states in ^{127}Cd have been identified with the ^{127}Cd ground state and the 283-keV isomer. Their respective half-lives have been measured to $0.45(^{12}_{8})$ s and 0.36(4) s. The experimentally observed β feeding to excited states of ^{127}In and the decay scheme of ^{127}In are discussed in conjunction with large-scale shell-model calculations.

DOI: 10.1103/PhysRevC.99.044310

I. INTRODUCTION

The heaviest doubly-magic nucleus far away from the line of stability accessible for experimental studies with today's techniques is ^{132}Sn. The region around it is not only a unique testing ground for nuclear structure models but also of significant relevance for the astrophysical rapid neutron capture process, the *r* process [1]. The *r* process is responsible for the production of about half of the elements heavier than iron. One of the main *r*-process abundance peaks is located at around $A = 130$. Sensitivity studies show that the nuclear properties of nuclei around the closed shells at $N = 50$, 82, and 126 have the largest impact on the *r*-process abundances [2–4]. In particular, β-decay half-lives, and therefore the contribution of first-forbidden β decays, have a direct impact on predicted abundance of rare-earth elements [2,5]. Since most of the nuclei involved in the *r* process are experimentally inaccessible, it is necessary to constrain theoretical models with reliable information on nearby nuclei to as accurately as possible predict relevant nuclear properties and thereby improve *r*-process simulations.

In this work, the high resolving power of JYFLTRAP [6] has been utilized to mass select ^{125}Cd and ^{127}Cd ions whose decays were then studied with the TASISpec decay station [7]. JYFLTRAP settings on ^{125}Cd as well as separately ^{125g}Cd and ^{125m}Cd served primarily methodological purposes. Here the focus is on ^{127}Cd and its β-decay daughter ^{127}In.

The first dedicated study on the β decay of ^{127}Cd was performed by Hoff *et al.* [8]. The reported decay scheme of ^{127}In suggested only one β-decaying state in ^{127}Cd with a half-life of $T_{1/2} = 0.43(3)$ s. Later studies identified two long-lived states with spin-parity assignments $I^\pi = 11/2^-$ and $I^\pi = 3/2^+$, respectively [9]. Recently, the excitation energy of the isomer in ^{127}Cd was measured to be 283.3(56) keV [10].

Although the existence of the long-lived $11/2^-$ and $3/2^+$ states has been confirmed for all odd-even cadmium nuclei from ^{121}Cd to ^{129}Cd [9], there is no experimental information on the ordering of these states in any of these nuclei. Based on systematics in the lighter isotopes, the $3/2^+$ state is assigned to the ground state for $121 \leqslant A \leqslant 125$ [11], whereas a crossing of the two states is expected between ^{127}Cd and ^{129}Cd [12]. Such a scenario is supported by recent shell-model calculations [13].

The work of Hoff *et al.* [8] and Arndt *et al.* [14] are the only studies providing γ-ray spectroscopic data on ^{127}In. Interestingly, more than half of the hitherto 43 γ-ray transitions associated with the decay could not be placed in the ^{127}In level scheme. The excitation energy of the $1/2^-$ isomer in ^{127}In, however, was fixed to $E_x = 408.9(3)$ keV [14,15]. The result agrees well with the value of 420(65) keV reported by Gausemel *et al.* [16]. A recent mass measurement yielded a consistent excitation energy of 390(18) keV [17]. In addition to the $1/2^-$ isomer, another β-decaying isomer at 1697(49) keV with a tentative spin-parity assignment of $I^\pi = 21/2^-$ and $T_{1/2} = 1.04(10)$ s has been identified [16,17]. Evidence for a short-lived, $T_{1/2} = 9(2)$ μs, high-spin isomer feeding this $21/2^-$ isomer has been found as well, with a tentative $29/2^+$ spin-parity assignment [18,19]. However, due to their high spin, these states are not populated by the ^{127}Cd β decay, and hence they are not relevant for the present work.

This work adds new insight into the level ordering of the $11/2^-$ and $3/2^+$ states in ^{127}Cd, their half-lives, and the excitation scheme of ^{127}In. Following a description of the experimental procedure, the obtained results are presented in detail, beginning with the derived level scheme of ^{127}In. Thereafter, the β decay of ^{127}Cd is discussed. The findings are then compared to extensive shell-model calculations.

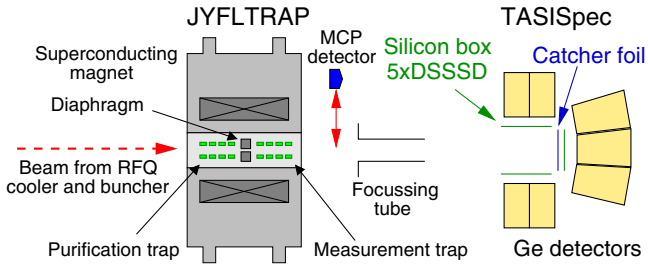

FIG. 1. Sketch of the experimental setup starting with the cooled and bunched beam from the RFQ cooler and buncher [22]. Using the purification trap [6] ^{127}Cd ions were separated from neighboring isobars, transferred to the TASISpec decay station [7], and deposited on an aluminum catcher foil. The measurement trap was employed for separating ground and isomeric state of ^{125,127}Cd. Dimensions are not to scale.

II. EXPERIMENT

The experiment was performed at the IGISOL facility at the University of Jyväskylä [6,20]. A 25-MeV proton beam provided by the K130 cyclotron impinging on a ^{nat}U target was used to produce Cd isotopes via proton-induced fission. After being stopped in the helium gas cell, the fission products were extracted using the sextupole ion guide SPIG [21] and accelerated to 30 kV. Using a 55° dipole magnet, singly-charged ions with mass number $A = 127$ were selected and guided toward the gas-filled radio-frequency quadrupole (RFQ) cooler and buncher [22]. Finally, the cooled and bunched ions were injected into the JYFLTRAP double-Penning-trap mass spectrometer [6]. In the purification trap, ^{127}Cd ions were selected via a mass-selective buffer gas cooling technique [23] using a 10-ms magnetron excitation pulse followed by a 90-ms quadrupolar excitation pulse at the ^{127}Cd cyclotron resonance frequency (846 636 Hz). A mass resolving power of $m/\Delta m = 53\,000$ was achieved, corresponding to $\Delta m/c^2 \approx 2.2$ MeV. This is sufficient to filter out neighboring isobars. The known μs isomer in ^{127}Cd [24] is too short lived and decays before reaching the Penning trap. The full trap cycle took ≈140 ms, which is roughly half of the previously reported half-life of ^{127}Cd [15]. This value was found to be the best compromise to allow for half-life measurements and collect sufficient statistics for β-γ(-γ) spectroscopy at the same time.

The isomeric ratio $\frac{^{127m}\mathrm{Cd}}{^{127gs}\mathrm{Cd}}$ in the beam delivered to TASISpec was estimated using the Phase-Imaging Ion-Cyclotron-Resonance (PI-ICR) [25] and time-of-flight ion-cyclotron-resonance [26,27] techniques, obtaining ratios of 5.3(7) and 2.6(8), respectively. A weighted average of 4.0(13) was used for the analysis.

Following their mass selection in JYFLTRAP, the ^{127}Cd ions were extracted, re-accelerated to 30 keV, and guided into the TASISpec decay station [7], see Fig. 1. The ^{127}Cd ions were deposited on a 9-μm-thick aluminum catcher foil placed 6 mm in front of a 0.52-mm-thick double-sided silicon strip detector (DSSSD) comprising $32 \times 32 = 1024$ pixels [7] on an active area of 58×58 mm^2. In addition, four pixelized 16×16, 0.97-mm-thick DSSSDs of the same size were placed upstream, effectively forming a compact cube of pixelized silicon charged-particle detectors. This silicon cube was placed inside a vacuum chamber with thin, 0.5-mm, aluminum windows toward four composite, high-purity germanium (HPGe) detectors: one former EUROBALL cluster detector [28] in the beam direction, two former EUROBALL clover detectors [29] to the left and right, as well as one clover detector with bismuth germanate anti-Compton shield from the GREAT spectrometer [30] facing the silicon box from below.

The signals from the silicon detectors as well as the anti-Compton shield were processed by custom-made 32-channel charge sensitive preamplifiers (CSP) [31] employing a 0.1-V/MeV range. Their read-out was handled by 14-bit 50-MHz sampling analog-to-digital converters (ADCs). These front-end boards with optical link extension (FEBEX) [32], were developed at the experiment electronics division of the Gesellschaft für Schwerionenforschung mbH (GSI), Darmstadt, Germany. Four commercial 16-bit 100-MHz SIS3302 sampling ADCs were used to process the HPGe-detector signals. A data acquisition system based on the GSI multi-branch system (MBS) [33] generated list-mode events comprising the recorded pulse shapes from the FEBEX system, energy and time of the HPGe-detector signals, as well as a time stamp for each trap release. The MBS was triggered by (i) a signal from a DSSSD strip above an energy threshold of ≈100 keV, (ii) a signal from at least two HPGe detectors within ≈5 μs and above an energy threshold of ≈20 keV, or (iii) a logic release signal from JYFLTRAP. A trigger on a single HPGe-detector signal was implemented as well. It was used for energy calibration and γ-ray detection efficiency measurements with standard, sealed γ-ray sources, e.g., ^{152}Eu, or combined conversion electron-γ sources such as ^{133}Ba or ^{207}Bi. The 1764.5- and 2614.5-keV γ-ray transitions in ^{214}Po and ^{208}Pb from natural background radiation were utilized as additional energy-calibration points beyond the range of the calibration sources. For higher γ-ray energies the energy calibration was extrapolated linearly. The γ-ray detection efficiency has been obtained using the Radware-EFFIT tool [34].

For the offline analysis of β-γ and β-γ-γ events a prompt-coincidence time window between the triggering silicon channel and the coincident HPGe-detector channel was implemented, reaching from ≈750 ns at 50 keV to ≈250 ns for energies above 1500 keV. To improve on γ-ray efficiency at high energies, so-called nearest-neighbor add-back of coincident events in adjacent Ge-detector crystals was performed. Events detected by the DSSSDs were only considered if the energy deposition was the same within ±1% in the n-side and p-side strips, also following an add-back procedure of coincident events in neighboring strips.

The spectroscopic results on the β decay of ^{127}Cd presented in the next section are primarily based on a 44-h-long measurement as described above, with about 7 to 10 mass-separated ^{127}Cd ions per second delivered from JYFLTRAP into TASISpec. In addition, the provision of clean beams out of JYFLTRAP of either the ground state of ^{125,127}Cd or their long-lived isomeric counterparts was attempted. Though in principle successful at the trap stage, the rate losses employing the Ramsey method [35,36] were too significant to allow for meaningful decay spectroscopy. On another attempt for ^{127}Cd,

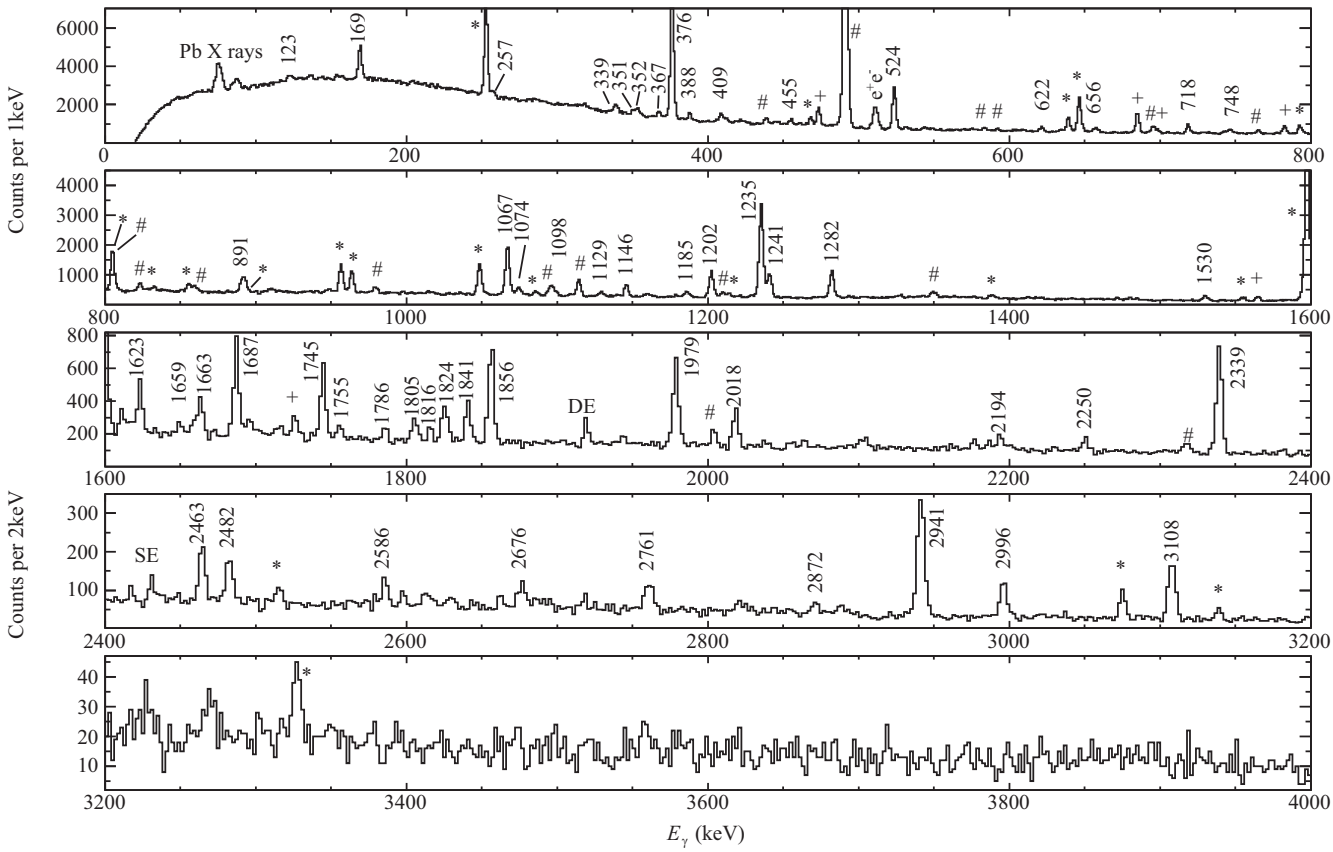

FIG. 2. Observed γ-ray spectrum of the ^{127}Cd β decay in prompt coincidence with a β particle. Known transitions emitted following the β decay of daughter nuclei are labeled with the following symbols: * for transitions in ^{127}Sn, # for transitions in ^{127}Sb, and + for transitions in ^{127}Te. Single- and double-escape peaks are denoted by SE and DE, and the corresponding annihilation peak at 511 keV is marked with (e^+e^-). The bin width is 1 keV for $E_\gamma \leqslant 1600$ keV and 2 keV for $E_\gamma > 1600$ keV. Energy labels are in keV.

using the phase-dependent cleaning method [37] based on the PI-ICR technique [25], some spectroscopic information could be obtained, but even in this case lack of statistics prevented a direct conclusion concerning the order of the β-decaying $3/2^+$ and $11/2^-$ states in ^{127}Cd [38].

III. RESULTS

The recorded γ-ray spectrum requiring a β particle in prompt coincidence is shown in Fig. 2. All observed γ-ray transitions could be identified to originate from either the β decay of the parent isotope ^{127}Cd or its daughter β emitters, ^{127}In, ^{127}Sn, or ^{127}Sb. For some high-energy transitions, single-escape and double-escape peaks are denoted as well. No γ-ray peaks could be attributed to known transitions in ^{126}In or ^{126}Sn, which could have been populated by β-delayed neutron emission. The measured relative transition intensities in the daughter nuclei ^{127}Sn, ^{127}Sb, and ^{127}Te are in agreement with previously reported yields [15] and it can be concluded that exclusively ^{127}Cd left JYFLTRAP and entered TASISpec.

Based on the known absolute transition intensities in ^{127}Sn after the β decay of either the ^{127}In $9/2^+$ ground state or the ^{127}In $1/2^-$ isomer, it was possible to determine their relative population, $\frac{N(^{127m}\mathrm{In})}{N(^{127g\mathrm{s}}\mathrm{In})} = 0.32(4)$, and an absolute transition yield of 24(3)% for the dominating 1235-keV ground-state transition in ^{127}In.

To unambiguously identify γ-ray transitions stemming from the β decay of ^{127}Cd, events detected in the first half of a trap cycle (i.e., within $\Delta t = [0, 70]$ ms after a trap-release trigger signal) were sorted in a "signal" spectrum, and those events detected in the second half of a trap cycle (i.e., $\Delta t = [70, 140]$ ms after a trap-release trigger signal and prior to the next trap release) were sorted in a "background" spectrum. Because of the relatively short half-life of ^{127}Cd and since the observed activity of the ^{127}Cd β decay is directly correlated to the trap-release signal, γ-ray peaks originating from the ^{127}Cd β decay will be less intense in the "background" spectrum than in the "signal" spectrum. This is different for the subsequent daughter decays: Their half-lives, ranging from a few seconds for ^{127}In to several days for ^{127}Sb, are significantly longer than the trap-release cycle of 140 ms. Hence their activity within a trap cycle will appear to be constant, and corresponding γ-ray peak-intensities in the "signal" and "background" spectrum will be the same. Subtracting the "background" spectrum from the "signal" spectrum will therefore remove all γ-ray peaks which are not correlated to the primary ^{127}Cd β decay. The resulting spectrum is shown in Fig. 3.

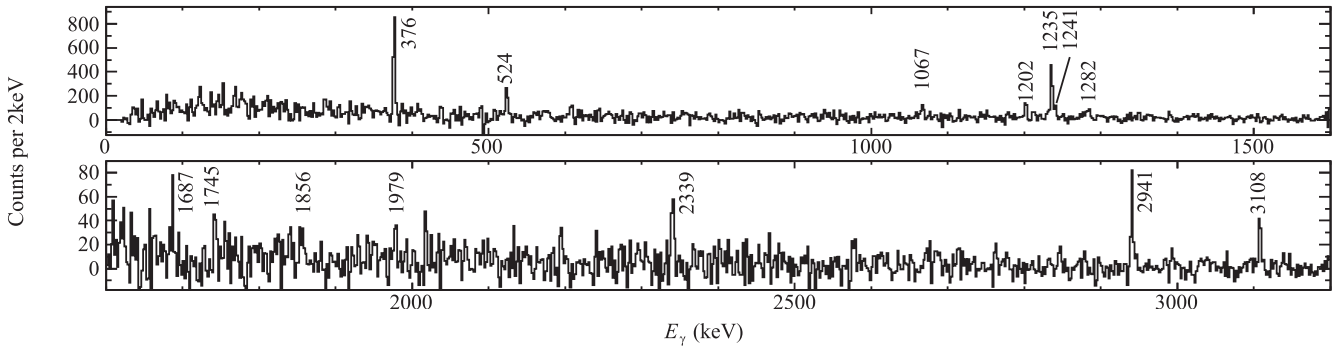

FIG. 3. Observed γ-ray spectrum for the first 70 ms after a trap-release signal where all γ rays detected later than 70 ms after the last trap-release signal were subtracted, i.e., highlighting γ-ray transitions following the first β-decay step of ^{127}Cd. Energy labels are in keV. See text for details.

A. The level scheme of ^{127}In

The proposed experimental level scheme of ^{127}In is shown in Fig. 4(b). Table I lists the measured energies and relative intensities as well as initial and final states of the 84 observed γ-ray transitions. The majority of these transitions were placed using β-γ-γ and β-γ-γ-γ information. The γ-ray peaks observed in Fig. 3 were used as a starting point since they can be firmly assigned to ^{127}In (see above). Of these 84 γ-ray transitions, 31 had been already identified in previous studies, of which only 17 had previously been placed in a level scheme of ^{127}In [8,14,15]. The placement of those γ-ray transitions agrees with the previously proposed decay scheme [8], with the exception of a 1979-keV line, which we position as a ground-state transition based on (non-)observed coincidence relations (see below). Some 13 unplaced γ-ray transitions reported by Hoff *et al.* [8] were not observed in the present study, which may find its explanation in the different production ratio between ^{127m}Cd and ^{127gs}Cd for the two

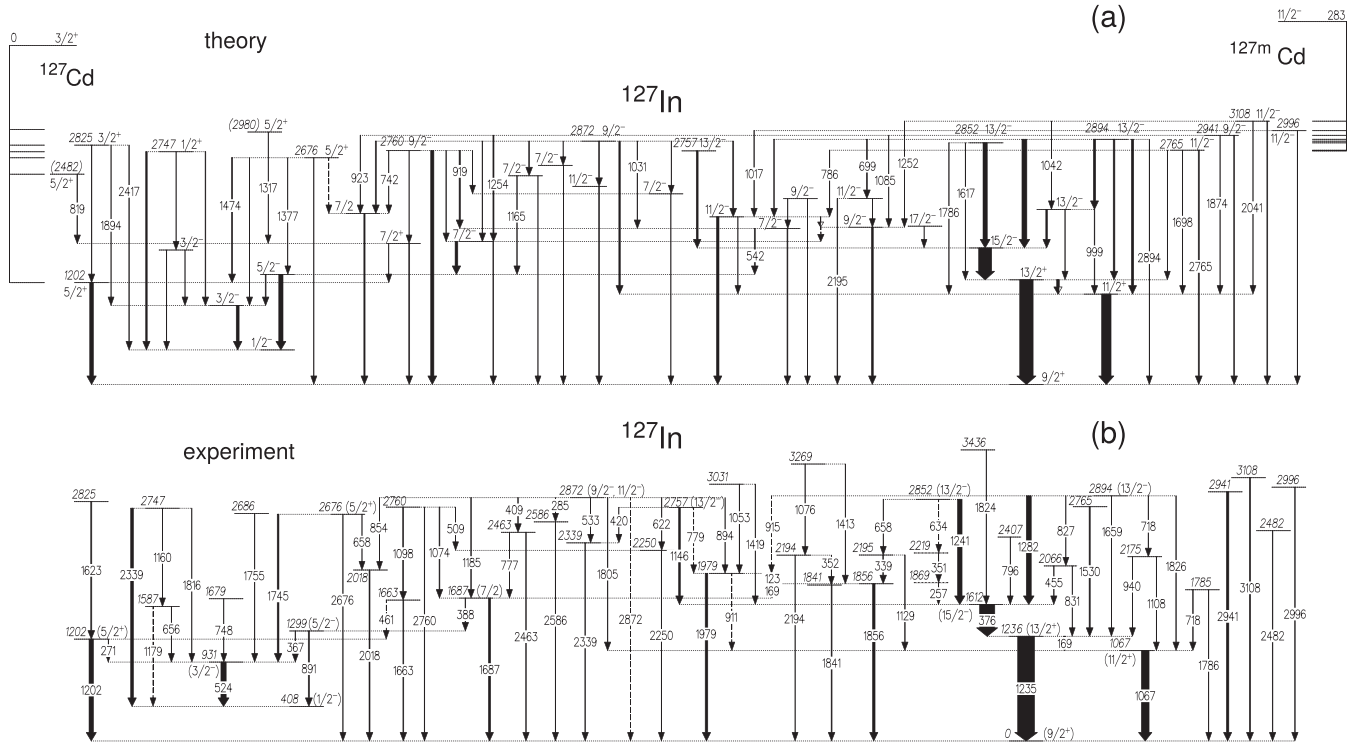

FIG. 4. Decay scheme of ^{127}In following the β decay of ^{127}Cd. Panel (a) shows the model based on shell-model calculations and panel (b) shows results observed experimentally. Energy labels are in keV, and tentative levels and transitions are dashed. In panel (a), the predicted main branches of Gamow-Teller (GT) β-decay feeding from ^{127}Cd are indicated for the $3/2^+$ ground state on the left-hand side and for the $11/2^-$ isomer on the right-hand side. This includes the excitation energies of the experimental levels associated with the main GT feeding. The γ-ray decay pattern in panel (a) is derived from experimental excitation energies but calculated transition strengths. Unobserved γ-ray transitions with predicted yields above the observational limit are labeled with their energy in keV. More details and the relevant discussion are provided in Sec. IV C. Detailed numerical results are given in Table IV.

TABLE I. Evaluated γ-ray energies E_γ; their relative γ-ray intensities from this work, I_γ, and previous studies, $I_\gamma^{\rm lit}$ [8]; initial and final states, E_i and E_f; and their proposed spin and parity assignments, J_i^π and J_f^π. Transitions marked with an asterisk cannot be placed unambiguously in the decay scheme and proposed initial and final states are in brackets. The absolute intensity per ^{127}Cd decay of the 1235.3-keV transition is 24(3)%.

E_γ (keV)	I_γ (%)[a]	$I_\gamma^{\rm lit}$ (%)[a]	E_i (keV)	E_f (keV)	J_i^π	J_f^π	E_γ (keV)	I_γ (%)[a]	$I_\gamma^{\rm lit}$ (%)[a]	E_i (keV)	E_f (keV)	J_i^π	J_f^π
122.9(3)	5.3(14)	3.6(5)	1978.6(2)	1855.9(2)			1097.7(5)	6.4(18)		2760.4(3)	1663.1(3)		
168.9(8)[b]	1.1(5)		1855.9(2)	1686.6(2)		(7/2)	1108.3(7)	1.6(4)		2175.3(3)	1066.5(1)		$(11/2^+)$
169.0(1)[c]	9.3(8)	15.0(10)	1235.5(1)	1066.5(1)	$(13/2^+)$	$(11/2^+)$	1128.9(3)	3.9(5)		2195.0(2)	1066.5(1)		$(11/2^+)$
257.4(3)[d]	2.7(6)		[1868.8(3)]	1611.5(2)		$(15/2^-)$	1145.7(2)	10.8(10)	8.5(20)	2757.3(2)	1611.5(2)	$(13/2^-)$	$(15/2^-)$
270.7(4)	0.7(2)		1202.2(3)	931.4(3)	$(5/2^+)$	$(3/2^-)$	1160.1(4)	1.6(5)	9.7(20)	2747.3(4)	1587.2(5)		
285.4(5)	1.4(5)		2871.9(2)	2586.3(4)	$(9/2^-)$		1179.0(8)	1.0(4)		1587.2(5)	408.0(3)		$(1/2^-)$
338.7(3)	5.1(8)	6.3(10)	2195.0(2)	1855.9(2)			1185.4(4)	4.9(5)		2871.9(2)	1686.6(2)	$(9/2^-)$	(7/2)
351.0(5)[d]	1.8(4)		[2219.3(4)]	[1868.8(3)]			1202.3(3)[e]	26.4(15)	54(3)	1202.2(3)	0	$(5/2^+)$	$(9/2^+)$
352.4(6)	<2		2193.6(4)	1840.9(3)			1235.3(2)[e]	100(4)	100(5)	1235.5(1)	0	$(13/2^+)$	$(9/2^+)$
367.2(3)	3.3(4)	8.7(20)	1298.6(3)	931.4(3)	$(5/2^-)$	$(3/2^-)$	1240.7(2)[e]	27.2(20)	27(5)	2852.3(2)	1611.5(2)	$(13/2^-)$	$(15/2^-)$
376.0(1)[e]	90(4)	90(5)	1611.5(2)	1235.5(1)	$(15/2^-)$	$(13/2^+)$	1282.1(3)[e]	29.4(16)	31(4)	2893.6(3)	1611.5(2)	$(13/2^-)$	$(15/2^-)$
388.1(3)	4.2(5)	8.3(20)	1686.6(2)	1298.6(3)	(7/2)	$(5/2^-)$	1413.4(7)	2.1(12)		3269.2(5)	1855.9(2)		
408.8(4)	4.6(6)		2871.9(2)	2463.3(3)	$(9/2^-)$		1419.4(6)	2.1(6)		3031.0(5)	1611.5(2)		$(15/2^-)$
419.5(5)	1.3(4)		2757.3(2)	2338.5(4)	$(13/2^-)$		1529.9(3)	6.9(7)		2765.4(3)	1235.5(1)		$(13/2^+)$
454.9(2)	3.5(4)		2066.4(2)	1611.5(2)		$(15/2^-)$	1622.9(5)	6.5(7)	17(3)	2825.1(6)	1202.2(3)		$(5/2^+)$
461.1(9)	0.5(2)		1663.1(3)	1202.2(3)		$(5/2^+)$	1659.1(8)	1.0(4)		2893.6(3)	1235.5(1)	$(13/2^-)$	$(13/2^+)$
509.3(9)	0.8(5)		2760.4(3)	2250.3(3)			1663.4(4)	5.2(6)	3.3(10)	1663.1(3)	0		$(9/2^+)$
523.5(2)[e]	31(2)	62(3)	931.4(3)	408.0(3)	$(3/2^-)$	$(1/2^-)$	1686.7(4)[(e)]	13.2(10)	11(3)	1686.6(2)	0	(7/2)	$(9/2^+)$
533.1(5)	1.3(4)		2871.9(2)	2338.5(4)	$(9/2^-)$		1744.7(4)[(e)]	10.3(9)	20.3(20)	2676.1(4)	931.4(3)	$(5/2^+)$	$(3/2^-)$
621.7(4)	2.5(15)		2871.9(2)	2250.3(3)	$(9/2^-)$		1755.0(4)	2.4(6)	6.0(10)	2686.4(5)	931.4(3)		$(3/2^-)$
633.6(6)[d]	1.5(6)		2852.3(2)	[2219.3(4)]	$(13/2^-)$		1785.6(7)	1.5(4)	10(2)	1785.0(3)	0		$(9/2^+)$
655.7(5)	2.3(6)	5.4(15)	1587.2(5)	931.4(3)		$(3/2^-)$	1805.2(4)	4.0(6)		2871.9(2)	1066.5(1)	$(9/2^-)$	$(11/2^+)$
657.7(5)[f]	2.2(7)		2852.3(2)	2195.0(2)	$(13/2^-)$		1815.9(6)	1.8(5)		2747.3(4)	931.4(3)		$(3/2^-)$
657.9(6)[g]	1.5(6)		2676.1(4)	2018.1(4)	$(5/2^+)$		1824.3(6)	2.4(5)		3435.8(5)	1611.5(2)		$(15/2^-)$
718.4(4)[h]	∼3.0		2893.6(3)	2175.3(3)	$(13/2^-)$		1826.1(8)	3.5(10)		2893.6(3)	1066.5(1)	$(13/2^-)$	$(11/2^+)$
718.4(4)[h]	∼4.3		1785.0(3)	1066.5(1)		$(11/2^+)$	1840.7(4)	5.5(7)		1840.9(3)	0		$(9/2^+)$
747.8(5)	1.6(5)		1679.2(6)	931.4(3)		$(3/2^-)$	1855.9(4)[(e)]	15.2(10)	14.5(20)	1855.9(2)	0		$(9/2^+)$
776.9(5)	1.5(6)		2463.3(3)	1686.6(2)		(7/2)	1978.6(4)[(e)]	15.5(10)	10(3)	1978.6(2)	0		$(9/2^+)$
779.2(8)	1.1(5)		2757.3(2)	1978.6(2)	$(13/2^-)$		2018.0(7)	6.0(7)		2018.1(4)	0		$(9/2^+)$
795.7(4)	1.5(3)		2407.2(4)	1611.5(2)		$(15/2^-)$	2193.8(5)	1.9(7)	5.1(15)	2193.6(4)	0		$(9/2^+)$
827.4(6)	1.7(3)		2893.6(3)	2066.4(2)	$(13/2^-)$		2250.2(6)	1.8(5)	3.3(15)	2250.3(3)	0		$(9/2^+)$
830.8(5)	1.6(6)		2066.4(2)	1235.5(1)		$(13/2^+)$	2338.8(7)[eh]	∼7.2		2338.5(4)	0		$(9/2^+)$
853.9(6)	0.9(5)		2871.9(2)	2018.1(4)	$(9/2^-)$		2339.3(7)[eh]	∼16	39(3)	2747.3(4)	408.0(3)		$(1/2^-)$
890.6(3)	7.8(15)		1298.6(3)	408.0(3)	$(5/2^-)$	$(1/2^-)$	2463.3(7)	4.5(7)		2463.3(3)	0		$(9/2^+)$
893.8(5)	1.8(6)		2871.9(2)	1978.6(2)	$(9/2^-)$		2482.4(5)*	4.0(10)	4.8(15)	[2482.4(5)]	[0]		$(9/2^+)$
911.3(8)	1.1(6)		1978.6(2)	1066.5(1)		$(11/2^+)$	2585.7(7)	2.6(6)		2586.3(4)	0		$(9/2^+)$
915.2(9)	1.3(6)		2893.6(3)	1978.6(2)	$(13/2^-)$		2676.1(6)	2.5(5)	12(2)	2676.1(4)	0	$(5/2^+)$	$(9/2^+)$
940.3(5)	1.9(7)		2175.3(3)	1235.5(1)		$(13/2^+)$	2760.5(6)	3.3(6)		2760.4(3)	0		$(9/2^+)$
1052.5(6)	2.4(13)		3031.0(5)	1978.6(2)			2871.8(9)	1.2(4)		2871.9(2)	0	$(9/2^-)$	$(9/2^+)$
1066.6(3)[e]	46(2)	61(8)	1066.5(1)	0	$(11/2^+)$	$(9/2^+)$	2941.3(5)[e*]	14.7(10)	17.5(20)	[2941.3(5)]	[0]		$(9/2^+)$
1073.5(5)	5.0(12)		2760.4(3)	1686.6(2)		(7/2)	2996.0(6)*	4.2(6)		[2996.0(6)]	[0]		$(9/2^+)$
1075.5(6)	2.3(2)		3269.2(5)	2193.6(4)			3107.9(6)[e*]	7.9(12)	8.9(15)	[3107.9(6)]	[0]		$(9/2^+)$

[a]Normalized with respect to I_γ(1235 keV).
[b]Energy and intensity based on the coincidence spectrum of the 1686.7-keV transition.
[c]Energy and intensity based on the coincidence spectrum of the 1066.6-keV and 376.0-keV transitions.
[d]Order of decay sequence uncertain. See text for details.
[e]Assignment to ^{127}Cd supported by time correlated spectra as described at the beginning of Sec. III.
[f]Energy and intensity based on the coincidence spectrum of the 1855.9-keV and 338.7-keV transitions.
[g]Energy and intensity based on the coincidence spectrum of the 2018.0-keV transition.
[h]Doublet structure. See text for details.

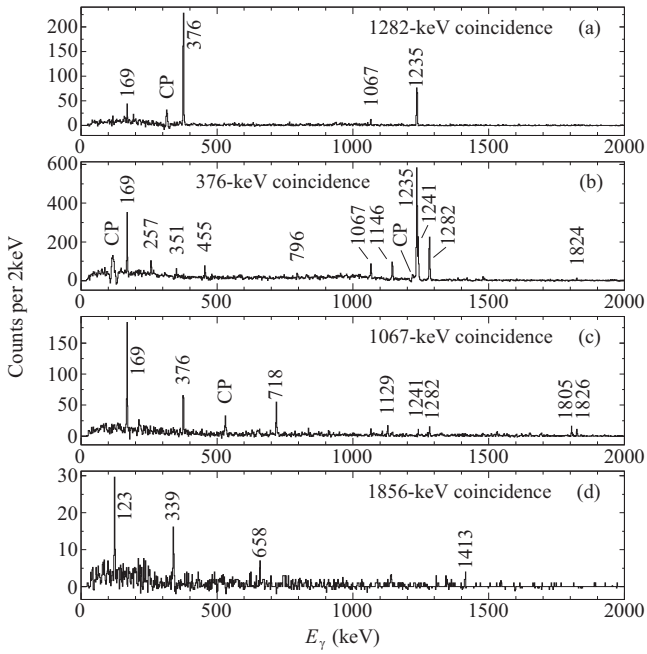

FIG. 5. Observed γ-ray spectra in prompt coincidence with (a) the 1282-keV transition, (b) the 376-keV transition, (c) the 1067-keV transition, and (d) the 1856-keV transition. Peaks marked with (CP) arise from Compton scattered γ rays of the intense 491-keV transition in ^{127}Sb, the 1235-keV transition in ^{127}In, or the 1597-keV transition in ^{127}Sn. In case of the spectrum shown in panel (a), for instance, the peak at ∼315 keV stems from 1597-keV γ rays which first deposited 1282 keV (315 keV) in one HPGe detector via Compton scattering and the remaining energy of 315 keV (1282 keV) in another HPGe detector. Energy labels are in keV.

experiments, which is discussed in Sec. III A 4 in more detail. The energies and the energy uncertainties of the excited states in ^{127}In were obtained using the Radware-xmgls tool [34].

1. Decay scheme on top of the 1235- and 1067-keV transitions

The structure consisting of the intense 169.0-, 376.0-, 1066.6-, 1145.7-, 1235.3-, 1240.7-, and 1282.1-keV transitions established by Hoff *et al.* [8] is confirmed by prompt β-γ-γ(-γ) coincidences. It relates to the right-hand side of the decay scheme shown in Fig. 4(b). The corresponding γ-ray coincidence relations are illustrated in Figs. 5(a)–5(c). All these transitions, with the exception of the 169.0-keV and 1145.7-keV transitions, are also visible in Fig. 3, clearly confirming their assignment to ^{127}In.

The spectrum in coincidence with the 1282.1-keV transition in Fig. 5(a) contains peaks at 169.0-, 376.0-, 1066.6-, and 1235.3-keV, establishing the state at 2893.6 keV. It is found that this state deexcites via a number of additional decay branches. For instance, the 454.9- and 827.4-keV transitions are in a cascade parallel to the 1282.1-keV line. There are direct 1659.1- and 1826.1-keV connections [cf. Fig. 5(c)] into the yrast $(13/2^+)$ and $(11/2^+)$ states, respectively. Parallel to these two transitions are weak 827.4-830.8-, 718.4-940.3-, and 718.4-1108.3-keV cascades.

Albeit being unresolved in the total γ-ray spectrum in Fig. 2, the transitions with the energies of 1824.3 and 1826.1 keV can be clearly distinguished by investigating the spectra in prompt coincidence with the 376.0-, 1235.3-, and 1066.6-keV transitions. The 1824.3-keV transition is observed in prompt coincidence with the 376.0- and 1235.3-keV transitions, placing it firmly on top of the state at 1611.5 keV. On the other hand, a 1826.1-keV transition is observed in prompt coincidence with the 1066.6-keV transition, directly populating the 1066.5-keV state as well as connecting to the well-established state at 2893.6 keV mentioned earlier.

The peak at 718.4 keV appears to be a doublet structure, too. The placements of the 940.3- and 1108.3-keV transitions depopulating a state at 2175.8 keV, which is fed by a 718.4-keV transition, is supported by coincidence information and the connectivity to the firm 2893.6-keV state. It can, however, not explain the relatively high coincidence yield of the 1066.6- and 718.4-keV transitions compared to the yield of the 1108.3- and 940.3-keV transitions in coincidence with the 1066.6-keV transition as shown in Fig. 5(c). This indicates feeding by another 718-keV transition to the 1066.5-keV state. A weak 1785.6-keV transition is observed in Fig. 2, which is not known in any of the daughter β decays. Hence we suggest a state at 1785.1 keV, depopulated by the 718.4- and 1785.6-keV transitions. Hoff *et al.* reported a 1785.6-keV transition as well, although with a considerably higher yield (cf. Table I), while they did not place it into their decay scheme. The intensity of the 718.4-keV transition feeding the 2175.8-keV state has been estimated by comparing the intensity of the 718.4- and 1235.3-keV peak in coincidence with the 940.3-keV transition, as well as the intensity of the 718.4- and 1066.6-keV peak in coincidence with the 1108.3-keV transition. The remaining intensity has been attributed to the 718.4-keV transition connecting the 1785.1- and 1066.5-keV states, such that the sum intensity corresponds to 7.3(7)% as measured in the β-γ spectrum. The energies of the two transitions have been determined using the coincidence spectra of the 940.3- and 1066.6-keV transitions for the transition depopulating the 2893.6- and 1785.1-keV states, respectively. In both cases the resulting transition energy is 718.4-keV, which in turn is equal the energy obtained from the β-γ spectrum.

The three transitions with the energies of 257.4, 351.0, and 633.6 keV (tentative) are observed in mutual coincidence as well as with the 376.0- and 1235.3-keV transitions. Therefore, they are placed as a cascade on top of the 1611.5-keV state, depopulating the state at 2852.3 keV, which is in turn established by the intense 1240.7-keV transition. The (tentative) order of the three weak low-energy transitions is based on their relative yields. The level at 2852.3 keV deexcites by several other paths. For example, the sequence 1855.9 [cf. Fig. 5(d)], 338.7, and 657.7 keV links to it, with the intermediate state at 2195.0 keV connected to the 1066.5-keV yrast level via the 1128.9-keV line. The 122.9-keV line seen in Fig. 5(d) connects the 1855.9-keV state with the one at 1978.6 keV. Several weak but parallel decay branches establish excited states at 1840.9, 2193.6, 3031.0, and 3269.2 keV.

The 1529.9-keV transition is seen in coincidence only with the 1235.3-keV ground-state transition, hence establishing a new level at 2765.4 keV. Similarly, the 795.7-keV transition

is placed straight on top of the 1611.5-keV level, since it is observed in coincidence with only the 376.0-keV and 1235.3-keV transitions.

The state at 3031.0 keV is established by a 1052.5-keV transition seen in prompt coincidence with the 1978.6-keV transition and supported by a 1419.4-keV transition in prompt coincidence with the 376.0-keV transition. Similarly, the state at 3269.2 keV is established by prompt coincidences between the 2193.8-keV and 1075.5-keV transitions and the 1855.9-keV and 1413.4-keV transitions [cf. Fig. 5(d)]. Because of their similar energy one could suggest that the 2195.0-keV state depopulated by the 338.7–1855.9 and 1128.9–1066.6 cascades is the same as the state that is depopulated by the observed 2193.8-keV transition and 352.4–1840.7 cascade. However, the 1075.5-keV transition could not be observed in prompt coincidence with either the 338.7-keV or the 1128.9-keV transition, and similarly there is no peak at 657.7 keV in prompt coincidence with the 2193.8-keV or the 352.4-keV transition. Furthermore, when assuming one state instead of the two states at 2193.6 keV and 2195.0 keV, then the energy differences between the obtained states were systematically too large (small) by ≈0.7 keV in case of the 352.4-, 1840.7-, and 2193.8-keV (1075.5- and 1128.9-keV) transitions. Hence we propose two states as shown in the level scheme in Fig. 4(b).

2. The states at 2757, 2760, and 2872 keV

The states at 2757.3, 2760.4, and 2871.9 keV represent the topmost states placed in the center of the decay scheme of ^{127}In in Fig. 4(b). The 2757.3-keV state deexcites predominately via the 1145.7-keV transition to the state at 1611.5 keV. Its position is furthermore supported by a weak 419.5-keV transition, which is seen in prompt coincidence with the 2338.8-keV transition.

The states at 2760.4 and 2871.9 keV are firmly established by many parallel, mostly two-step, cascades. Both these states decay into the state at 1686.6 keV. Besides the intense transition into the $(9/2^+)$ ground state, this state also deexcites via the 388.1-keV transition into the states connected to the low-spin, negative-parity $(1/2^-)$ isomer located at 408.0 keV (cf. Sec. III A 3). Several of the involved ground-state transitions were reported by Hoff *et al.* [8] but were not placed into the level scheme (see Table I).

Solely in prompt coincidence with the 1066.6-keV transition, the 1805.2-keV transition connects to the prominent 2871.9-keV state as well. In fact, a total of eight transitions are found to deexcite this state in the present work, but no γ-ray transition is observed feeding it. Thus, this state, like several others at about 3 MeV excitation energy, is a prime candidate for direct (Gamow-Teller) β feeding.

3. Structures connected to the 408-keV $(1/2^-)$ isomer

The majority of the observed transitions feeding the $(1/2^-)$ isomer have already been reported by Hoff *et al.* [8]. However, only the 367.2-, 523.5-, 655.7-, 1744.7-, and 1755.0-keV transitions were placed into the level scheme. Based on the coincidence information and relative intensities obtained in this experiment, we confirm these placements, as can be seen from Fig. 6(b).

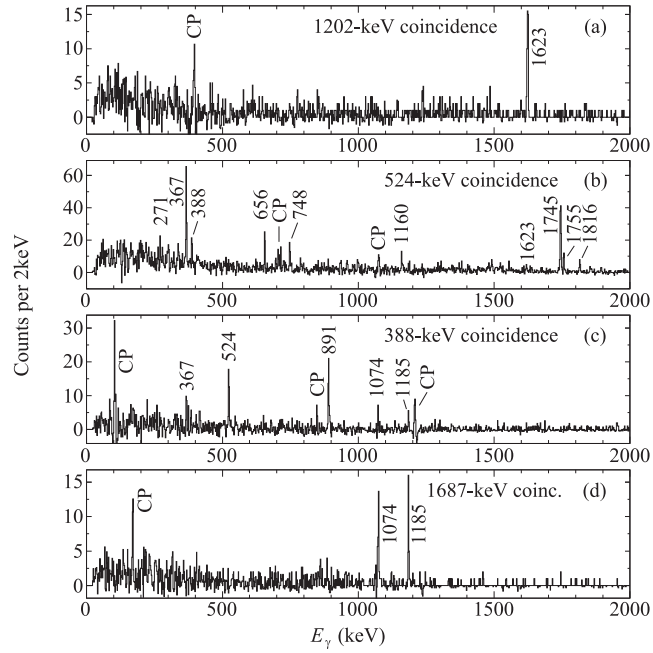

FIG. 6. Observed γ-ray spectra in prompt coincidence with (a) the 1202.3-keV transition, (b) the 523.5-keV transition, (c) the 388.1-keV transition, and (d) the 1686.7-keV transition. Peaks marked with CP are due to Compton scattered γ rays as explained in Fig. 5. Energy labels are in keV.

Hoff *et al.* [8] also assigned the 388.1-keV transition to ^{127}In. We clearly see several γ-ray peaks in coincidence with this transition, which are identified with the 367.2-, 523.5-, 890.6-, 1073.5-, and 1185.4-keV transitions in Fig. 6(c). The latter two transitions are firmly placed on top of the 1686.6-keV state, as described above, since they are observed in prompt coincidence with the 1686.7-keV transition, the coincidence spectrum of which is displayed in Fig. 6(d).

The 890.6-keV line is naturally placed as the "$E2$ crossover" parallel to the 367.2- and 523.5-keV transitions, since it is *not* observed in coincidence with either of these and corresponds to the sum of their energies. After the position of the isomer has been fixed with the help of the 388.1-keV transition, we can confirm the suggestions by Arndt *et al.* [14]. First, they observed a weak peak at 270.2 keV and tentatively assigned it to ^{127}In deexciting a state at 1202 keV. In this work we also observe a very weak peak at 270.7 keV in prompt coincidence with the 523.5-keV transition, as shown in Fig. 6(b), connecting the 1202.2-keV state with the level at 931.4-keV. Second, Arndt *et al.* [14] suggested that the γ-ray transitions with the energies of 1744.7 and 2677.4 keV (as well as 1755.4 and 2688.6 keV) observed by Hoff *et al.* [8] stem from the same state, the former feeding the 931.4-keV state and the latter the ground state. In our work, two γ-ray transitions at 1744.7 and 1755.0 keV are observed in prompt coincidence with the 523.5-keV transition. Together with the 2676.1-keV γ-ray transition and another, parallel, 657.9-2018.0-keV branch, a state at 2676.1 keV is estab-

lished. Note that a 853.9-keV line connects the intermediate state at 2018.1 keV with the 2871.9-keV level discussed in the previous section. A ground-state transition deexciting the 2686.4-keV state, which is established by the 1755.0-keV transition, is most likely below our sensitivity, considering that Hoff *et al.* [8] observed that the 2688.6-keV transition is much weaker than the 2677.4-keV transition.

A 1815.9-keV transition in coincidence with the 523.5-keV transition establishes the state at 2747.3 keV, supported by a 655.7-1160.1-keV coincidence in parallel. The energy difference between the 2747.3-keV state and the isomer, 2339.3 keV, is very similar to the 2338.8-keV transition mentioned earlier in Sec. III A 2. The observed intensity of the 2339-keV peak in Fig. 2 is 23.1(18)%, less than the previously reported intensity of 39(3)% [8]. Considering the γ-ray yields observed in this work and by Hoff *et al.* [8] (see Sec. III A 4), it seems that this peak indeed is a doublet, partly fed by the decay of the ^{127}Cd $11/2^-$ state and partly by the decay of the ^{127}Cd $3/2^+$ state. Based on the different γ-ray yields discussed in Sec. III A 4 we can estimate the intensity of the transition populating the isomer and ground state to $\sim$16% and 7.2%, respectively. The individual transition energies were estimated by fitting the 2339-keV peak in Fig. 2 with the intensity ratio of the two contributions being fixed.

The 1622.9-keV transition is only seen in coincidence with the 1202.3-keV ground-state transition, confirming its placement by Hoff *et al.* [8]. Being only observed in coincidence with the 523.5-keV transition, the 747.8-keV establishes a new state at 1679.2 keV.

As can be seen in the ^{127}In decay scheme in Fig. 4(b), the position of the $(1/2^-)$ isomer is fixed by several transitions connecting it to established states, such as the 1202.2-, 2676.1-, and the 1686.6-keV states. The resulting excitation energy of the $(1/2^-)$ isomer is 408.0(3) keV. This is in very good agreement with the value of 408.9(3) keV suggested by Arndt *et al.* [14,15] and recent mass measurements, which reported an excitation energy of 390(18) keV [17].

4. γ-Ray yield considerations

The observed intensities for transitions around the 1236-keV and 1612-keV states agree very well with those reported by Hoff *et al.* [8]. In both cases the intensity of the 1235-keV transition serves as normalization.

A minor disagreement is seen for the 169- and 1067-keV transitions, for which we observe a somewhat lower relative yield. More interestingly, however, in our work the measured yields of the 367-, 388-, 524-, 656-, 1160-, 1202-, and 1623-keV transitions are only roughly half of those reported by Hoff *et al.* A possible explanation is that these two regions of the decay scheme are populated predominantly by the decay of the ^{127}Cd $3/2^+$ state in the levels in connection with the 408-keV, $(1/2^-)$ isomer in ^{127}In and the ^{127}Cd $11/2^-$ state in the states around the 376-keV transition. The differences in the observed intensities can be readily explained by a significantly larger fraction of ions in the $11/2^-$ state in the ^{127}Cd beam of the present experiment due to the different reaction mechanism used. Our experiment was based on proton-induced fission, while in the experiment conducted by Hoff *et al.* the ^{127}Cd nuclei were produced by thermal-neutron-induced fission of $^{\text{nat}}$U. In fact, in studies investigating fission yields of ^{238}U and ^{232}Th [39,40], it was observed that the population of high-spin isomers is favored in proton-induced fission and that the trend increases with increasing incident proton energies. Thus, it seems very plausible that during the experiment conducted by Hoff *et al.* the ^{127}Cd $3/2^+$ state was populated about twice as much as in our work.

Consequently, it is straightforward to conclude that transitions for which the measured yield is roughly the same as reported by Hoff *et al.* are populated by the decay of the ^{127}Cd $11/2^-$ state, i.e., those shown on the right-hand side of the proposed level scheme in Fig. 4(b), and that those with about half the relative yield reported by Hoff *et al.* are predominantly populated by the decay of the ^{127}Cd$3/2^+$ state, i.e., those shown on the left-hand side in Fig. 4(b).

The placement of the four transitions with the energies of 2482.4, 2941.3, 2996.0, and 3107.9 keV is difficult because there are no transitions observed in coincidence. Since the observed intensities of these transitions are similar to the previously reported intensities, we propose to place these transitions as ground-state transitions, most likely populated by the decay of the ^{127}Cd $11/2^-$ state. Their shell-model interpretation is discussed in Sec. IV.

5. Spin-parity considerations

For the two states at 1067 and 1236 keV above the $(9/2^+)$ ground-state spin-parity assignments of $(11/2^+)$ and $(13/2^+)$ were already proposed by Scherillo *et al.* [19] based on systematics from neighboring isotopes. The 1612-keV state deexcites exclusively via the 376-keV transition to the $(13/2^+)$ state at 1236 keV. For spins below 15/2 or a spin-parity assignment of $15/2^+$ one expects additional transitions to, for instance, the $(11/2^+)$ 1067-keV state or the ground state. Since the 1612-keV state shows no sign of isomerism either, the possible spin-parity options are limited to $15/2^-$ and $17/2^+$.

The 2894-keV state has γ-ray transitions connecting to the 1612-keV state as well as the $(13/2^+)$ 1236-keV and $(11/2^+)$ 1067-keV states. It has no γ-ray feeding from higher-lying states. Therefore, the 2894-keV state has to be populated by the ^{127}Cd $11/2^-$ β decay, assuming a Gamow-Teller (GT) character (cf. Sec. III B). That in turn restricts the possible spin-parity assignment to $9/2^-$, $11/2^-$, and $13/2^-$. A $9/2^-$ assignment can be excluded because of the observed 1659-keV transition to the $(13/2^+)$ state at 1236 keV. At the same time it excludes the $17/2^+$ option for the 1612-keV state. Therefore, we tentatively assign a spin-parity of $(15/2^-)$ to the 1612-keV state. Considering that we do not observe an intense direct $(E1)$ γ-ray transition from the state at 2894 keV to the ground state, we propose a tentative spin-parity of $(13/2^-)$ for the 2894-keV state. With a similar line of arguments we can narrow down possible spin-parties for the 2757 and 2852-keV states: Both states have a strong transition to the $(15/2^-)$ 1612-keV state and no feeding from higher-lying states. Hence, these states have to be populated by the ^{127}Cd $11/2^-$ β decay, again assuming a GT character (cf. Sec. III B). As in the case of the 2894-keV state, the possible

spin-parity assignments are thereby limited to $9/2^-$, $11/2^-$, and $13/2^-$. Due to the absence of intense direct ($E1$) γ-ray transitions to the ground state, we suggest a spin and parity of $(13/2^-)$ for both the 2757- and 2852-keV states.

Similarly to the 1067- and 1236-keV states, the two states at 931 and 1299 keV indicate a yrast sequence on top of the 408-keV $(1/2^-)$ isomer. Referring to the systematics in lighter odd-mass cadmium isotopes [15], we therefore propose spin-parities of $(3/2^-)$ and $(5/2^-)$ to the 931- and 1299-keV states, respectively. Consequently, the 1202-keV state has to be of $5/2^+$ or $7/2^-$ nature, since it has prompt γ-ray transitions connecting to the ground state and to the $(3/2^-)$ state at 931 keV. We furthermore observe significant β feeding into the 1202-keV state, as can be seen in Table II. Considering a GT β decay of the $3/2^+$ or $11/2^-$ state in ^{127}Cd, a spin-parity of $7/2^-$ can be ruled out. Therefore, the 1202-keV state corresponds most likely to the $5/2^+$ yrast state, partially fed by the β decay of the $3/2^+$ state in ^{127}Cd. Similarly to the 1202- and 271-keV transitions in case of the 1202-keV state, the 2676- and 1745-keV transitions connect the 2676-keV state to the ground state and the 931-keV state. Together with the large observed β feeding to the 2676-keV state, we can follow the same line of arguments as for the 1202-keV state and propose a spin and parity of $(5/2^+)$ for the 2676-keV state, too. Note that the feeding of the 1202- and 2676-keV state by the β decay of the $3/2^+$ state in ^{127}Cd is also consistent with the γ-ray yield considerations discussed earlier.

The prompt 1805-keV γ-ray transition links the 2872-keV state with the $(11/2^+)$ state at 1067 keV, constraining the possible spins for the 2872-keV state between 7/2 and 15/2. As in the case of the 2894-keV state, the 2872-keV state must be populated by the ^{127}Cd $11/2^-$ β decay, which—assuming GT character—limits possible spin-parity assignments to $9/2^-$, $11/2^-$, and $13/2^-$. The 1687-keV state has prompt γ-ray transitions to the $(9/2^+)$ ground state as well as to the $(5/2^-)$ state at 1299 keV. On the other hand, the 1185-keV transition connects this state with the 2872-keV state, which has possible spin-parities of $9/2^-$, $11/2^-$, or $13/2^-$. Therefore, we tentatively assign a spin of (7/2) to the 1687-keV state and $(9/2^-)$ or $(11/2^-)$ to the 2872-keV state. However, a spin-parity of $9/2^-$ for the 1687-keV state as well as a $13/2^-$ for the 2872-keV state cannot be ruled out.

B. The β decay of ^{127}Cd

As a consequence of the tentative spin-parity assignments made in the previous section, the states connected to the 931-keV state as well as the state at 2825 keV are considered to be populated by the β decay of the $3/2^+$ state in ^{127}Cd. The majority of all the other states are either part of a two-step cascade connecting the $(9/2^-)$ state at 2872 keV and the $(9/2^+)$ ground state or they have a direct γ-ray transition connecting to a state with a spin larger than 9/2. Therefore, we consider them to be populated primarily in the course of the β decay of the $11/2^-$ state in ^{127}Cd. The β feeding of these states amounts to considerably more than 50% as can be seen in Table II. Since the fraction of ^{127}Cd ground state in the beam is only about 20% (cf. Sec. II) one can firmly conclude that the $11/2^-$ state in ^{127}Cd corresponds to the isomer and the ^{127}Cd ground state to the $3/2^+$ state.

TABLE II. The energies, E_x, of excited states in ^{127}In populated in the β decay of ^{127}Cd; proposed spin-parity assignments; the observed β-feeding intensities, I_{β^-}; the individual β-feeding intensities from the $11/2^-$ state, $I_{\beta^-}(11/2^-)$, and the $3/2^+$ state, $I_{\beta^-}(3/2^+)$; as well as the resulting log ft values. Tentative states are in brackets.

E_x (keV)	I^π	I_{β^-} (%)	$I_{\beta^-}(11/2^-)$ (%)	$I_{\beta^-}(3/2^+)$ (%)	log ft
0.0	$(9/2^+)$	<18	<22		>5.5
408.0(3)	$(1/2^-)$	<15		<75	>5.0
931.4(3)	$(3/2^-)$	2.1(7)		10(4)	5.7(2)
1066.5(2)	$(11/2^+)$	4.4(9)	5.5(11)		5.9(1)
1202.2(3)	$(5/2^+)$	4.8(8)		24(4)	5.2(1)
1235.5(2)	$(13/2^+)$	<4	<5		>5.8
1298.6(3)	$(5/2^-)$	1.7(5)		8(3)	5.6(2)
1587.2(5)		0.4(2)		2.1(11)	6.2(3)
1611.5(2)	$(15/2^-)$	2.5(13)	3.1(16)		6.0(2)
1663.1(3)		<0.4	<0.5		>6.7
1679.2(6)		0.38(13)		1.9(7)	6.2(2)
1686.6(2)	(7/2)	1.2(5)	1.4(6)		6.3(2)
1785.0(3)		1.4(2)	1.7(3)		6.2(1)
1840.9(3)		1.1(3)	1.4(3)		6.2(1)
1855.9(2)		<1.7	<2.1		>6.1
[1868.8(3)]		(<0.5)	(<0.6)		(>6.6)
1978.6(2)		3.7(8)	4.7(10)		5.7(1)
2018.1(4)		0.9(3)	1.1(4)		6.3(2)
2066.4(2)		0.8(2)	1.0(3)		6.3(2)
2175.3(3)		<0.4	<0.5		>6.6
2193.6(4)		<0.4		<2	>6.0
2195.0(2)		1.6(4)	2.0(5)		6.0(1)
[2219.3(5)]		(<0.3)	(<0.4)		(>6.7)
2250.3(3)		<0.2	<0.3		>6.8
2338.5(3)		1.1(2)	1.4(3)		6.1(1)
2407.2(4)		0.36(9)	0.45(11)		6.6(1)
2463.3(3)		<0.7	<0.9		>6.2
[2482.4(5)]		[1.0(3)]	[1.3(4)]		[6.1(2)]
2586.3(4)		0.3(2)	0.4(2)		6.6(3)
2676.1(4)	$(5/2^+)$	3.4(6)		17(3)	4.9(1)
2686.4(5)		0.58(16)		2.9(8)	5.7(2)
2747.3(4)		4.7(6)		23(3)	4.7(1)
2757.3(2)	$(13/2^-)$	3.2(5)	3.9(6)		5.5(1)
2760.4(3)		3.7(8)	4.6(10)		5.4(1)
2765.4(3)		1.7(3)	2.1(4)		5.8(1)
2825.1(6)		1.6(3)		7.7(15)	5.2(1)
2852.3(2)	$(13/2^-)$	7.4(11)	9.3(14)		5.1(1)
2871.9(2)	$(9/2^-)$	5.4(9)	6.8(11)		5.2(1)
2893.6(3)	$(13/2^-)$	9.6(13)	12.0(17)		5.0(1)
[2941.3(5)]		[3.5(5)]	[4.4(6)]		[5.4(1)]
[2996.0(6)]		[1.0(2)]	[1.3(3)]		[5.9(1)]
3031.0(5)		1.1(4)	1.4(5)		5.8(2)
[3107.9(6)]		[1.9(4)]	[2.4(5)]		[5.6(1)]
3269.2(5)		1.1(4)		5(2)	5.2(2)
3435.8(5)		0.58(14)	0.72(18)		6.0(1)

The half-lives of both the $3/2^+$ and $11/2^-$ states of ^{127}Cd were determined by first selecting events involving γ rays associated with these decays and then studying their time distribution with respect to the latest trap-release signal. In-

tense γ-ray peaks that can be firmly associated with the β decay of the $11/2^-$ state stem from the 169-, 376-, 1067-, 1146-, 1235-, 1241-, and 1282-keV transitions (cf. Fig. 4), with the 376-keV transition contributing most of the statistics. If only β decays in prompt coincidence with the 376-keV transition are considered, one obtains a half-life of $T_{1/2} = 0.32(^{5}_{4})$ s. Investigating the time distribution of detected β decays which are in prompt coincidence with at least one of the aforementioned γ-rays results in a consistent half-life result of $T_{1/2} = 0.36(4)$ s.

Likewise, the half-life of the $3/2^+$ state can be determined to $T_{1/2} = 0.45(^{12}_{8})$ s, which is slightly longer than the half-life measured for the $11/2^-$ state. Here β decays in prompt coincidence with the 524-, 1202-, 1623-, or 1745-keV transitions are taken into account. In this case the statistics contributed from the 524-keV peak dominates the result. Consistently, a half-life of $T_{1/2} = 0.49(^{26}_{13})$ s is obtained when analyzing only β decays in prompt coincidence with the 524-keV transition.

The two half-lives for the $11/2^-$ state and $3/2^+$ state are in agreement with previously reported values of 0.30(3) s [41], 0.37(7) s [15], and 0.43(3) s by Hoff *et al.* [8] and 0.33(2) s reported by Lorusso *et al.* [2]. However, all of the hitherto reported measurements did not distinguish between the $3/2^+$ and $11/2^-$ states of ^{127}Cd. In fact, the difference in the values reported by Hoff *et al.* and Lorusso *et al.* can be explained by the different reaction mechanisms used to produce ^{127}Cd. In the latter experiment ^{127}Cd was produced via in-flight fission of a 345 MeV/u ^{238}U beam impinging on a beryllium target. This favors the population of the $11/2^-$ state, resulting in a half-life value that agrees more with the half-life we obtain for the $11/2^-$ state than with the half-life we determine for the $3/2^+$ state.

Based on the estimated relative population of the ^{127}In isomer and its ground state as well as the absolute γ-ray transition intensities (see Sec. III), it is possible to estimate the β feeding to each state in ^{127}In as the intensity difference of populating and depopulating γ-ray transitions of a given excited state. Table II lists the energies, tentative spin-parity assignments, and the estimated β feeding for the observed states in ^{127}In. As discussed in Sec. III A 5, one can correlate each state with the β decay of either the $3/2^+$ or the $11/2^-$ state in ^{127}Cd. In conjunction with the measured ratio of ^{127}Cd isomer and ground state in the beam (see Sec. II), the individual β-decay branching ratios for these two states are calculated in Table II. In the last column of Table II the corresponding $\log ft$ values are listed, calculated using the LOGFT code [42] with the half-lives discussed earlier, a Q value of $Q_\beta = 8149(24)$ keV [43], and an excitation energy of 283.3(56) keV [10] for the $11/2^-$ isomer.

The $\log ft$ values 4.9 and 4.7 for the 2676- and 2747-keV states, respectively, indicate decays of GT character. Similar values are reported for lighter odd-mass In isotopes [44,45] and for ^{129}In, where $\log ft$ values of 4.5 and 4.7 were measured [13]. The states with the strongest β feedings after the decay of the ^{127}Cd $11/2^-$ state have $\log ft$ values of 5.0 to 5.2. These are comparable to those obtained for the ^{123,125}In isotopes [44,45] but significantly higher than the $\log ft$ value of 4.2 reported in Ref. [13] for the heavier odd-mass ^{129}In isotope. A number of states have $\log ft$ values around 6, which indicates that first-forbidden (ff) transitions compete with GT decays. The β feeding into the $(1/2^-)$ isomer, the $(3/2^-)$ and $(5/2^-)$ yrast states, for example, have $\log ft$ values of $>5.0, 5.7$, and 5.6, which is very similar to those obtained in the neighboring ^{129}In [13]. These decays could be driven by ff transitions of the type $\nu d_{3/2} \rightarrow \pi(p, f_{5/2})$, as already suggested in Ref. [13]. Likewise, the $(9/2^+)$ ground state with a lower limit of $\log ft > 5.5$ is most likely populated by the decay of the $11/2^-$ state in ^{127}Cd via the ff transition $\nu h_{11/2} \rightarrow \pi g_{9/2}$. For the same decay in ^{125}Cd and ^{129}Cd lower limits of $\log ft > 5.9$ [45] and $\log ft > 5.3$ [13] were reported.

Note, however, that the observed β-decay feedings, and hence the $\log ft$ values, are subject to weak and therefore not observed γ-ray transitions, the "pandemonium effect" [46]. In particular, the β-decay feedings to states at higher excitation energies above $\sim$2.5 MeV are likely to be underestimated because of unobserved, weak, γ-ray transitions deexciting these states. This would lead to reduced $\log ft$ values in turn. On the other hand, the β-decay feedings to lower-lying states could be overestimated because of unobserved weak γ-ray transitions feeding these states. This applies especially to the ground and isomeric states.

IV. SHELL-MODEL CALCULATIONS AND DISCUSSION

Shell-model calculations have been performed using the code NuShellX [47,48]. For the region of interest, ^{132}Sn is used as the doubly-magic closed core. The $Z = 28$ to 50 region, comprising the $f_{5/2}$, $p_{3/2}$, $p_{1/2}$, and $g_{9/2}$ proton shells, is considered for proton holes. Similarly, the $N = 50$ to 82 space, comprising the $g_{7/2}$, $d_{5/2}$, $d_{3/2}$, $s_{1/2}$, and $h_{11/2}$ neutron shells, is accessible for neutron holes. Two sets of interactions have been investigated: The "jj45" interaction, made available via the NuShellX package, comprises two-body matrix-elements based on a G-matrix formalism and has single-particle energies adjusted for the ^{132}Sn region (see, e.g., Ref. [49]). The second interaction, denoted "NA-14," is based on the CD-Bonn nucleon-nucleon potential renormalized by means of the $V_{\mathrm{low}-k}$ approach [50]. The neutron single-particle energies are taken from Ref. [51]. The proton single-particle energies are taken from recent mass measurements [52] and spectroscopic information on $A = 129$ Cd and In isotopes [53,54]. Furthermore, a few two-body matrix-elements have been adjusted as outlined in, for instance, Refs. [13,54,55].

With the above, an assessment of the interactions based on prominent states in ^{125,127,129}Cd and ^{125,127,129}In is conducted in Sec. IV A. Thereafter, the GT strengths and the associated GT feeding pattern from the $3/2^+$ ground state and the $11/2^-$ isomer in ^{127}Cd into ^{127}In is discussed in Sec. IV B. A generic quenching factor of 0.75 was applied to the GT matrix elements according to, for example, Refs. [56,57], in line with a similar discussion in Ref. [13].

Finally, in Sec. IV C a predicted ^{127}In decay scheme is derived [cf. Fig. 4(a)], which is based on the experimental ^{127}Cd beam composition in conjunction with predicted major GT β feeding into ^{127}In levels as well as observed excitation energies in combination with predicted $B(M1)$, $B(E2)$, and $B(M2)$ relative transition strengths. Standard effective charges

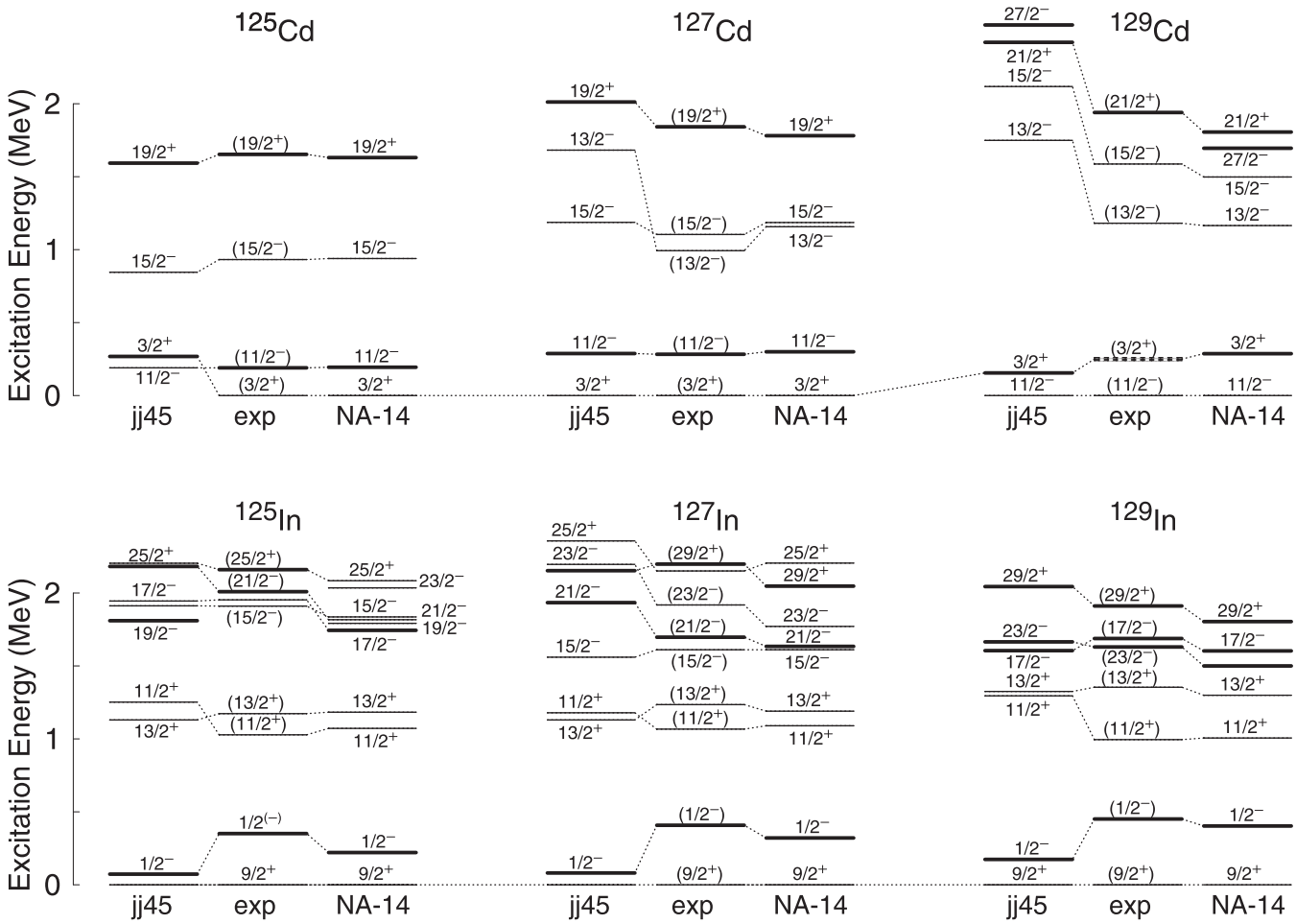

FIG. 7. Comparison of experimental (exp) and calculated (jj45 and NA-14) level energies for the $A = 125$, 127, and 129 isotopes of Cd (top row) and In (bottom row). Isomeric states are marked by thick horizontal lines. The energy of the excited $(3/2^+)$ state in ^{129}Cd (dashed) is experimentally not yet determined. Thin dashed lines connect observed and predicted energy levels. With the exception of the jj45 prediction of ^{125}Cd, the $3/2^+$ (^{125,127}Cd), the $11/2^-$ (^{129}Cd), and $9/2^+$ (all three In isotopes) ground states served for normalization. See text for more details.

of $e_{\mathrm{eff},p} = 1.5$ and $e_{\mathrm{eff},n} = 0.5$ are used to calculate $B(E2)$ strengths [56], as well as 70% of the free g-factor values for $B(M1)$ strengths. While $B(M2)$ strengths are rarely competitive in prompt γ-ray spectroscopy, one has to account for $B(E1)$ strengths. Since they are formally forbidden in the employed shell-model space, they need to be inferred "by hand," here with a generic transition strength of $B(E1) = 5 \times 10^{-5}\ e^2\ \mathrm{fm}^2$.

A. Level energy systematics

Figure 7 shows a comparison of experimental (exp) and calculated (jj45 and NA-14) level energies for a number of odd-A isotopes ($A = 125$, 127, and 129) of Cd in the top row and In in the bottom row, respectively. In each case, a selection of states is shown, primarily experimentally known isomeric states, indicated by thick horizontal lines in the figure, as well as some high-spin states through which some of these isomers decay, i.e., states which are experimentally rather well established. The experimental sequences are based on information available in evaluated nuclear structure data files (ENSDF) [15,45,58] and relevant publications on ^{125}Cd [10,59–62], ^{127}Cd [2,9,10,24,61], ^{129}Cd [9,12,13,54], ^{125}In [17,19], ^{127}In [17,19], and ^{129}In [13,16,19].

Concerning the spins and parities of the $9/2^+$ ground states and $1/2^-$ first-excited states in the In chain, both models agree with the order of the experimental results or propositions, with the somewhat more optimized NA-14 interaction providing a better description of the energetics. Sums of seniority $v = 1$ partitions in the corresponding wave functions are provided in Table III. They expectedly increase toward the shell closure at $N = 82$, with the NA-14 interaction calling generally for purer wave functions. Similar trends are seen for the $11/2^-$ and $3/2^+$ states in the Cd chain. However, while the experimentally evidenced switch between $3/2^+$ ground state and $11/2^-$ isomer between ^{127}Cd and ^{129}Cd is correctly reproduced by both interactions, jj45 predicts another switch toward ^{125}Cd, which is in disagreement with the observations.

Both interactions reproduce nicely the observed $11/2^-$–$15/2^-$–$19/2^+$ sequences in ^{125}Cd and ^{127}Cd, with the $19/2^+$ state being predicted isomeric due to the demand of a slow electromagnetic $M2$ transition. In all predictions the

TABLE III. Sums of partitions (%) of selected wave functions; "any" indicates that any nucleon pair may be in any possible j shell within the available model space.

Seniority	I^π	Configuration	Isotope	NA-14	jj45
$v=1$	$9/2_1^+$	$\pi(g_{9/2})^{-1}$	^{125}In	59	43
			^{127}In	60	47
			^{129}In	87	56
	$1/2_1^-$	$\pi(p_{1/2})^{-1}$	^{125}In	73	49
			^{127}In	74	53
			^{129}In	76	58
	$11/2_1^-$	$\nu(h_{11/2})^{-1}$	^{125}Cd	56	42
			^{127}Cd	61	51
			^{129}Cd	64	63
	$3/2_1^+$	$\nu(d_{3/2})^{-1}$	^{125}Cd	54	41
			^{127}Cd	54	45
			^{129}Cd	86	78
$v=3$	$13/2_1^-$	$\nu(\text{any})^{-2}_{1,2}\nu(h_{11/2})^{-1}$	^{127}Cd	26	31
		$\pi(\text{any})^{-2}_2\nu(h_{11/2})^{-1}$	^{127}Cd	40	19
	$21/2_1^+$	$\pi(g_{9/2})^{-1}\pi(p_{1/2})^{-1}\nu(h_{11/2})^{-1}$	^{129}Cd	98	95
	$11/2_1^+$	$\pi(g_{9/2})^{-1}\nu(\text{any})^{-2}_2$	^{125}In	66	53
			^{127}In	68	51
			^{129}In	67	53
		$\pi(g_{9/2})^{-1}\nu(\text{any})^{-2}_4$	^{125}In	26	29
			^{127}In	24	28
			^{129}In	25	27
	$21/2_1^-$	$\pi(g_{9/2})^{-1}[\nu(h_{11/2})^{-1}\nu(d_{3/2})^{-1}]_6$	^{127}In	54	40
		$\pi(g_{9/2})^{-1}[\nu(h_{11/2})^{-1}\nu(d_{3/2})^{-1}]_7$	^{127}In	21	19

yrast $17/2^-$ or $19/2^-$ levels are calculated to lie above the $19/2^+$ state. Interestingly, however, NA-14 and jj45 differ significantly on the location of the yrast $13/2^-$ state in ^{127}Cd: NA-14 places it correctly close to and below the $15/2^-$ state, while jj45 puts it several hundreds of keV too high. In terms of wave-function composition, jj45 predicts far fewer (19%) $\pi(\text{any})^{-2}_2\nu(h_{11/2})^{-1}$ partitions than NA-14 (40%), i.e., fewer than what one typically associates with "$J=2$ collectivity" in the shell-model picture.

A similar effect is seen in the predictions for ^{129}Cd, where the energy gap between the $11/2^-$ ground state and, e.g., the $13/2^-$ and $15/2^-$ excited states, is predicted to be much larger for the jj45 interaction compared with NA-14. The latter interaction describes the energetics of ^{129}Cd very well. A β-decaying $27/2^-$ state located at $E_x \approx 1700$ keV is predicted, as already pointed out in Ref. [55]. The only possible partition of that $27/2^-$ state is a fully aligned, seniority $v=3$ $\pi(g_{9/2})^{-2}_8\nu(h_{11/2})^{-1}$ configuration. Similarly, the fully aligned $\pi(g_{9/2})^{-1}\pi(p_{1/2})^{-1}\nu(h_{11/2})^{-1}$ partition accounts for almost 100% of the wave function of the $21/2^+$ state in ^{129}Cd, which is predicted to be isomeric irrespective of whether the $27/2^-$ state were located just below or just above it. Its preferred electromagnetic decay proceeds toward the yrast $15/2^-$ state in any case, as discussed in detail in Ref. [54].

Assessing the predictions for the odd-A In isotopes in the bottom row of Fig. 7, one can note a problem with the jj45 interaction in consistently overestimating the position of the yrast $11/2^+$ level. The underlying problem is similar to the one noted above for the $13/2^-$ levels in the Cd chain but now related to too-little $J=2$ neutron pair content.

The experimentally established $17/2^-$, $23/2^-$, and $29/2^+$ isomers in ^{129}In [16] are well reproduced by both calculations. Here the flip between the $17/2^-$ and $23/2^-$ states is not particularly worrysome, because the levels lie close in energy, on the order of mean-level deviations for appropriate shell-model calculations. The three isomers find their explanation in energetically favored, (anti)aligned $v=3$ configurations such as $[\pi(g_{9/2})^{-1}\nu(h_{11/2})^{-1}]_{10}\times\nu(d_{3/2})^{-1}_{\pm 3/2}$ ($17/2^-$ and $23/2^-$ isomers, respectively), as well as $[\pi(g_{9/2})^{-1}\nu(h_{11/2})^{-2}_{10}]_{29/2}$ ($29/2^+$ isomer).

For ^{127}In, the very same aligned $v=3$, $29/2^+$-configuration gives rise to a predicted $29/2^+$ isomer, in full agreement with experimental knowledge [19]. Both calculations, however, fail to predict the suggested decay path through the yrast $25/2^+$ state, in line with Fig. 5 in Ref. [19]. Furthermore, jj45 also places the yrast $23/2^-$ above the $29/2^+$, which in that case would be β decaying, at variance with the observations. Finally, both calculations predict an isomeric $21/2^-$ state, now settled at an excitation energy of 1697(49) keV [17]. In comparison with ^{129}In, this single isomer is seemingly replacing the $17/2^-$-$23/2^-$ "isomeric doublet." In case of ^{125}In, the experimental results concerning a high-spin isomer at 2161 keV are debated (see, for instance, Sec. IV in Ref. [19], at variance with the evaluation in Ref. [45]). In Fig. 7 we propose $25/2^+$ for that state based on our calculations, which by no means predicts an isomeric $23/2^-$ state, because it would have too many options to decay via fast $M1$ or $E2$ transitions to lower-lying negative-parity states. Second, only minor changes in NA-14 parameters can alternate the order of the closely lying multiplet of $15/2^-$, $17/2^-$, $19/2^-$, and $21/2^-$ states, such that a decay sequence as illustrated in Fig. 4 of Ref. [19] appears most reasonable.

Concluding this section, the NA-14 parametrization provides an overall excellent prediction and explanation for observed (isomeric) states in odd-A Cd and In isotopes in the region of interest. Therefore, for the more comprehensive assessment of the low-lying β-decaying states of ^{127}Cd and the observed ^{127}In γ-ray decay scheme below, we continue to work only with the NA-14 interaction.

B. Gamow-Teller strengths

Figure 8(a) shows the calculated GT strength distribution for the β decay of the $11/2^-$ state in ^{127}Cd to excited states in ^{127}In. The GT resonance is predicted between 2.8 and 3.5 MeV. The states which are most strongly populated in this GT decay are those which comprise the largest partitions of $\pi(g_{9/2})^{-1}\nu(g_{7/2})^{-1}(\text{any})^{-3}$ configurations. This is expected since the only possible GT transition within the considered model space is the $\nu g_{7/2}\rightarrow\pi g_{9/2}$ single-particle transition. For the $11/2^-$ state in ^{129}Cd, for instance, it is observed that around 50% of the β-feeding intensity feeds a single $(13/2^-)$ state whose calculated wave function comprises a 92% partition of the $\pi(g_{9/2})^{-1}\nu(g_{7/2})^{-1}(h_{11/2})^{-1}$ configuration [13]. In the case of the ^{127}Cd β decay the calculated

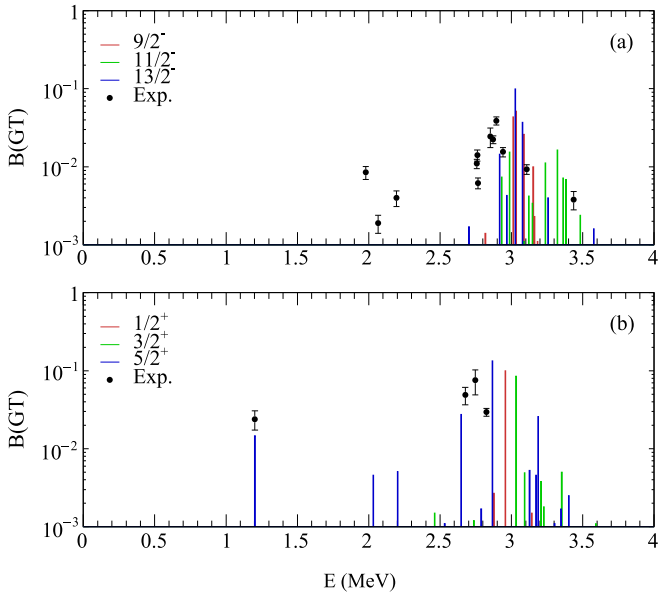

FIG. 8. Results of shell-model calculations for the Gamow-Teller strength distribution, B(GT), for the decay of the $11/2^-$ (a) and the $3/2^+$ (b) states in ^{127}Cd to excited states in ^{127}In. The experimental GT strengths are shown as black dots.

3027-keV $13/2^-_9$ state receives the strongest GT feeding and comprises around 50% $\pi(g_{9/2})^{-1}\nu(g_{7/2})^{-1}(\text{any})^{-3}$ configurations. This state can be associated with the experimentally observed $(13/2^-)$ state at 2894 keV. In fact, by comparing calculated and experimentally observed decay patterns as well as β-feeding intensities, it is possible to identify a number of observed states with predicted $9/2^-$, $11/2^-$, and $13/2^-$ states, as discussed in Sec. IV C. The experimentally deduced GT strength distribution B(GT) for these states reveals a very similar distribution [see Fig. 8(a)], shifted by around 150–200 keV to lower excitation energies.

Similarly well reproduced are the prominent features of the GT distribution of the $3/2^+$ ^{127}Cd β decay. Here the experimentally observed states at 2676, 2747, and 2825 keV can be identified with the $5/2^+_8$ 2841-, $1/2^+_3$ 2928-, and $3/2^+_4$ 3005-keV states, also some 150–200 keV above the experimental observation. These states comprise a 50%, 78%, and 67% partition of the $\pi(g_{9/2})^{-1}\nu(g_{7/2})^{-1}(d_{3/2})^{-1}(h_{11/2})^{-2}$ configuration, respectively. The measured β feeding into the yrast $(5/2^+)$ state at 1202 keV is remarkably well described by the calculated GT transition strength.

C. Level scheme of ^{127}In

In the previous sections, very good to excellent agreement between experimental observations and shell-model calculations with the NA-14 parametrization is found. This initiated an attempt to model the observed decay scheme of ^{127}In shown in Fig. 4(b), which resulted in the predicted decay scheme displayed in Fig. 4(a). More details can be assessed in Table IV

The predictions are based on the following procedure: (i) Experimentally, the sum of relative yields of all γ-ray transitions reaching either the $(9/2^+)$ ground state of ^{127}In ($\approx$270 intensity units according to Table I) or its $(1/2^-)$ isomeric state ($\approx$60 intensity units) is determined, i.e., a $\sum I_\gamma = 330$ is set. (ii) A 4:1 ratio of $11/2^-$ isomeric vs. $3/2^+$ ground-state portion is set for the ^{127}Cd beam delivered from JYFLTRAP (see Sec. II), i.e., the $3/2^+$ ground state is supposed to feed 20% of 330 intensity units into ^{127}In, and the $11/2^-$ isomer 80% of 330 intensity units. (iii) Predicted states in ^{127}In are identified which carry the major GT strengths from the two states in ^{127}Cd. In Fig. 4(a), these entry points are indicated on the very left- and very right-hand side for the GT decay of the $3/2^+$ and $11/2^-$ mother states in ^{127}Cd, respectively. In case of the $3/2^+$ GT decay, these are the $5/2^+_1$ (11%), $5/2^+_5$ (7.2%), $5/2^+_8$ (29%), $1/2^+_3$ (20%), $3/2^+_4$ (16%), and $5/2^+_{12}$ (4.3%) states, in total 88% of the respective GT strength [see Fig. 8(b)]. In case of the $11/2^-$ GT decay, the relevant states are the $13/2^-_7$ (4.2%), $11/2^-_9$ (4.2%), $9/2^-_{10}$ (12%), $13/2^-_9$ (26%), $9/2^-_{11}$ (14%), $13/2^-_{10}$ (9.5%), $9/2^-_{12}$ (6.6%), $11/2^-_{14}$ (2.5%), and $11/2^-_{15}$ (3.4%) ones, accounting for 82% of that GT strength [see Fig. 8(a)]. (iv) The GT feeding is renormalized to the ^{127}Cd beam content and the observed total of 330 γ-ray intensity units, i.e., both the remaining small GT branches as well as any other β-decay mode are neglected. The corresponding numbers of GT feeding intensities used for the modeling are given in the rightmost column of Table IV. (v) Experimental values for the excitation and γ-ray energies are used for the electromagnetic phase-space factor to determine γ-ray branching ratios. (vi) Level by level, the most suitable match between observed and predicted state is evaluated, based as usual on excitation energies, but here primarily on β and γ feeding *and* γ-decay pattern. (vii) Gamma-ray transitions with intensities above 0.5 intensity units ($E_\gamma = [100, 500]$ keV) or 1.0 intensity units ($E_\gamma > 500$ keV) are displayed in Fig. 4(a).

There is a striking visual correspondence between the two decay schemes shown in Fig. 4—despite the simplifications listed above and the use of one generic $B(E1)$ strength for all parity changing, $\Delta I \leqslant 1$, transitions. In particular, all major decay branches (thick γ-ray lines) are perfectly well reproduced, and almost all observed levels find a proper theoretical counterpart. Interestingly, the modeled sum of γ-ray yields into the $9/2^+$ ground state and the $1/2^-$ isomer is practically identical to the measured values, though the γ-ray flux is far from simple, i.e., parts of the flux originating from the $11/2^-$ GT β decay reaches the $1/2^-$ isomer and vice versa; for instance, the 1202-keV $5/2^+_1 \rightarrow 9/2^+$ ground-state transition.

A binding energy shift (BES) of -64 keV, a mean-level deviation (MLD) of 97 keV, and a mean branching deviation (MBD) of 0.12 [63] derived from 38 levels are indicators of an excellent agreement between experiment and shell-model theory. In terms of BES and MLD values, the main, and in a sense one and only, discrepancy between experiment and theory lies in the fact that the excitation energies of the many states around 3 MeV fed directly by GT transitions are calculated some 150–200 keV higher in energy with respect to experiment. As mentioned earlier, one common characteristic of these states are significant contributions of partitions comprising one neutron hole in $\nu(g_{7/2})$. Hence, a modification of the $\nu(g_{7/2})$ SPE might improve the predicted excitation energies of the states which are directly fed by

GT transitions. The MBD value could be further improved by adjusting $B(E1)$ strengths for individual transitions, which is mentioned for a few specific cases below. For the overall picture, however, this is neither required nor wanted.

Starting on the left-hand side of Fig. 4, the levels at 931, 1202, 1299, 1663, and 1687 keV are interpreted as yrast $3/2^-_1$, $5/2^+_1$, $5/2^-_1$, $7/2^+_1$, and $7/2^-_1$ states. The $5/2^+$ state defines itself via distinct predicted and observed direct GT feeding. The predicted 271-keV $5/2^+_1 \rightarrow 3/2^- E1$ transition is too weak to be included in the modeled decay scheme, while a doubled $B(E1)$ strength would account for it. Looking at the 1687-keV $7/2^-_1$ state, the predicted ratio between the 388- and 1687-keV transitions is seemingly at variance with experiment, but also in this case a slight increase of $B(E1)$ strength would easily change the ratio in favor of the 1687-keV ground-state $E1$ transition.

Besides the 1202-keV state, those observed at 2676 keV ($5/2^+_8$), 2747 keV ($1/2^+_3$), and 2825 keV ($3/2^+_4$) can be associated with direct GT feeding. The latter provides an explanation for the 1623-keV connection to the 1202-keV state. The 2747-keV state is defined by the 2339-, 1816-, and 1160-keV decay pattern. In turn, the 1160-keV transition suggests that the 1587-keV level should correspond to the $3/2^-_2$ state, supported by its own 656- and 1179-keV decays. The observed state at 1679 keV is only very weakly connected to the GT decay pattern. An interpretation as $3/2^-_3$ appears favorable (cf. Table IV).

The remaining two states predicted to be directly fed by GT strengths from the $3/2^+$ ground state of ^{127}Cd are not observed experimentally. At first glance, the excitation energy of the 2482-keV level as well as the nonobservation of any feeding γ rays point toward it representing the above-mentioned $5/2^+_5$ state. However, the predictions for this state and the $5/2^+_{12}$ state, at an estimated excitation energy of 2980 keV, indicate dominating γ-ray decays into the 1663-keV, $7/2^+_1$ yrast level but not into the $9/2^+$ ground state.

The GT strength of the $11/2^-$ isomer in ^{127}Cd proceeds mainly to three $9/2^-$, three $11/2^-$, and three $13/2^-$ states, all located in a rather small excitation energy region between 2.75 and 3.10 MeV. Each of these three spin groups, or "triplets," shows a rather similar and characteristic γ-ray decay pattern. The three $13/2^-$ levels are predicted to reveal intense, dominant, and rather pure $M1$ decays to the yrast $15/2^-$ level observed at 1612 keV. The respective γ rays are the ones at 1146, 1241, and 1282 keV, which in turn define the association between the three predicted $13/2^-$ levels and those observed at 2757, 2852, and 2894 keV. The distinction between the latter two is based on the presence of the 827, 1659, and 1826-keV transitions depopulating the level at 2894 keV. In addition, the decay sequence via the 827-keV line suggests to match the observed level at 2066 keV with the predicted yrast $13/2^-_1$ state.

Different from the $13/2^-$ multiplet, the decay of the three states belonging to the $9/2^-$ multiplet is predicted to be highly fragmented with up to 10 transitions passing the observational limit. In turn, this considerably eases the matching for at least two of three, because the experimental levels at 2760 keV and especially at 2872 keV are found to decay by many γ-ray transitions, in line with such predictions. The seemingly too-intense 2760-keV ground-state decay could once again be adjusted with a modified, in this case reduced, $B(E1)$ strength. The third $9/2^-$ state is associated with the experimental state at 2941 keV. Since its GT feeding is predicted a factor of two less than for the other two $9/2^-$ states, one cannot expect to see many of the thus weak γ-ray decays in our experiment.

In conjunction with selected transitions from the $13/2^-$ states defined earlier, the myriad of connections cascading down to the $9/2^+$ ground state allows us to identify matches for essentially all intermediate states: the 1841-, 1856-, 1979-, 2194-, and 2195-keV levels can be interpreted as the $7/2^-_2$, $9/2^-_1$, $11/2^-_1$, $9/2^-_2$, and $11/2^-_2$ states. The feeding and decay pattern of the somewhat higher-lying levels at 2250, 2339, 2463, and 2586 keV match best the predicted $7/2^-_4$, $11/2^-_4$, $7/2^-_6$, and $7/2^-_8$ states. There is only one state which deserves special attention, namely the one at 2018 keV. It is shown in Fig. 4 and listed in Table IV as $7/2^-_3$, while it almost equally well could be associated with the predicted $7/2^+_3$ state. The latter would be fed by the (therefore dashed) 658-keV transition, while the 854-keV decay into it, for example, should be absent.

With both the $9/2^-$ and $13/2^-$ "GT triplet" assigned, there are three levels left for the respective $11/2^-$ "GT triplet": those at 2765, 2996, and 3108 keV. Experimentally, all of them reveal one exclusive γ-ray decay—the latter two a direct, stretched $E1$ to the $9/2^+$ ground state, while the 2765-keV level decays via the 1530-keV transition to the 1236-keV $13/2^+$ yrast level. The predictions are such that all three $11/2^-$ states should have a significant branch to the ground state, and in addition a few other transitions to one or another intermediate state, though primarily to the yrast $11/2^+$ level at 1067 keV. Since the GT feeding to the $11/2^-$ triplet (32 intensity units) is small in comparison to the respective $9/2^-$ (101 units) and $13/2^-$ (137 units) states, the majority of the transitions other than the ground-state $E1$ transitions are predicted close to the observational limit. The presence of the 1530-keV $11/2^-_9 \rightarrow 13/2^+_1$ transition rather than the 2765-keV $E1$ (cf. Fig. 2) ground-state transition may be explained by a specifically favorable $E1$ matrix element between the 2765- and 1236-keV states.

The levels observed at 1785, 1869, and 2175 keV are found to be only weakly connected to the GT-based decay pattern, though they can be associated rather well with predicted $13/2^+_2$, $17/2^-_1$, and $13/2^+_4$ states (see Table IV). The levels observed at 2407, 3031, 3269, and 3436 keV could not be assigned. They probably belong to weak GT branches or relate to first forbidden β decays from the $11/2^-$ isomer in ^{127}Cd.

V. CONCLUSIONS

Utilizing the mass resolution power of JYFLTRAP and the nuclear decay station TASISpec, the β decay of ^{127}Cd has been studied in detail. The individual half-lives of the $3/2^+$ and $11/2^-$ β decaying states in ^{127}Cd are reported for the first time. The order of the two states could be established by comparing γ-ray yields from Ref. [8] and data presented in this article. Furthermore, the level scheme of ^{127}In has been substantially extended, comprising 43 excited states connected by 84 γ-ray transitions.

The results have been confronted with extensive shell-model calculations, employing an empirically optimized interaction. The calculated GT strength distribution of the ^{127}Cd β decay in combination with the calculated level energies and γ-ray branching ratios in ^{127}In reproduce the observed ^{127}In decay scheme remarkably well. It therefore confirms that the β decay of ^{127}Cd is primarily driven by the $\nu g_{7/2} \rightarrow \pi g_{9/2}$ GT transition. Despite the good agreement assuming only GT transitions, ff transitions directly populating the ^{127}In $9/2^+$ ground state and $1/2^-$ isomeric state might play a role.

ACKNOWLEDGMENTS

The authors thank the accelerator staff at the University of Jyväskylä. This work is supported by the European Union's Horizon 2020 research and innovation programme Grant No. 654002 (ENSAR2), the Swedish Research Council (VR 2013-4271), the Knut and Alice Wallenberg foundation (KAW 2015.0021), the Academy of Finland under the Finnish Centre of Excellence Program (Nuclear and Accelerator Based Physics Research at JYFL 2012-2017), and the Spanish Ministerio de Economía y Competitividad under Contract No. FPA2017-84756-C4-2-P. The support from the Academy of Finland under Grants No. 275389, No. 284516, No. 312544, and No. 295207 is acknowledged. A.K. and L.C. acknowledge the funding from the European Union's Horizon 2020 research and innovation program under Grant No. 771036 (ERC CoG MAIDEN). U.F. acknowledges support from the Birgit and Hellmuth Hertz Foundation of the Royal Physiographic Society in Lund. Ch.L., L.G.S., and D.R. would like to thank B. A. Brown, H. Grawe, and C. Qi for support concerning the shell-model calculations.

APPENDIX

For completeness and in order to support the findings presented in the main article, the detailed results of the shell-model calculations discussed in Sec. IV and their comparison to the experimentally observed states are provided in Table IV.

TABLE IV. Comparison between calculated and associated experimentally observed states in ^{127}In populated in the β decay of the ground state (predicted $I^\pi = 3/2^+$) and isomeric state (predicted $I^\pi = 11/2^-$ at $E_x = 300$ keV, experimentally at $E_x = 283(6)$ keV [17]) of ^{127}Cd. The association of observed and predicted states is based on energy and, primarily, β-feeding and γ-ray decay branches, as well as tentatively assigned experimental spins and parities and yrast arguments. For the parameters of the shell-model calculation, see Sec. IV of the main article. $E1$ transitions, forbidden in the model space, are accounted for with a generic reduced transition strength of $B(E1) = 5 \times 10^{-5}\ e^2\,\mathrm{fm}^2$. A total of 38 calculated levels are associated with experimental counterparts, which gives rise to a binding energy shift of BES $= -64$ keV, a mean-level deviation of MLD $= 97$ keV, and an overall mean branching deviation of MBD $= 0.12$ [63]. The normalization of the predicted relative γ-ray intensities, $I_{\gamma,\mathrm{theo}}$, is based on the sum of the intensities of all observed γ-ray transitions, $I_{\gamma,\mathrm{exp}}$, feeding either the $9/2^+$ ground state or the $1/2^-$ isomeric state in ^{127}In (326 units according to Table I of the main article).

$E_{x,\mathrm{exp}}$ (keV)	$E_{x,\mathrm{theo}}$ (keV)	τ_{theo} (ps)	J_i^π ($\hbar$)	J_f^π ($\hbar$)	E_γ (keV)	$I_{\gamma,\mathrm{exp}}$ (%)	$I_{\gamma,\mathrm{theo}}$ (%)	b_{exp} (%)	b_{theo} (%)	MBD$_i$	$I_{GT,\mathrm{theo}}$ (%)
408	321	n/a[a]	$1/2_1^-$	β^-							
931	936	0.39	$3/2_1^-$	$1/2_1^-$	524	31(2)	17	100	100	n/a	
1067	1090	0.09	$11/2_1^+$	$9/2_1^+$	1067	46(2)	56	100	100	n/a	
1202	1174	4.3	$5/2_1^+$	$9/2_1^+$	1202	26(2)	22	97(1)	99	0.018(5)	8.0
				$3/2_1^-$	271	0.7(2)	0.2	3(1)	1		
1236	1190	3.6	$13/2_1^+$	$9/2_1^+$	1235	100(4)	79	91(1)	83	0.082(21)	
				$11/2_1^+$	169	9.3(8)	16	9(1)	17		
1299	1281	9.3	$5/2_1^-$	$9/2_1^+$	1299	n.o.[b]	0.6		2	0.090(30)	
				$1/2_1^-$	891	7.8(15)	25	70(6)	81		
				$3/2_1^-$	367	3.3(4)	5.2	30(6)	17		
1587	1653	0.59	$3/2_2^-$	$1/2_1^-$	1179	1.0(4)	1.7	30(13)	51	0.096(60)	
				$3/2_1^-$	656	2.3(6)	1.5	70(13)	47		
				$5/2_1^+$	385	n.o.	0.0		0		
				$5/2_1^-$	288	n.o.	0.1		2		
1612	1611	240	$15/2_1^-$	$11/2_1^+$	544	n.o.	0.0		0	0.000(20)	
				$13/2_1^+$	376	90(4)	77	100	100		
1663	1645	0.07	$7/2_1^+$	$9/2_1^+$	1663	5.2(6)	5.8	91(4)	89	0.017(7)	
				$11/2_1^+$	596	n.o.	0.0		0		
				$5/2_1^+$	461	0.5(2)	0.7	9(4)	11		
				$5/2_1^-$	364	n.o.	0.0		0		
1679	1799	0.30	$3/2_3^-$	$1/2_1^-$	1271	n.o.	0.5		26	0.106(65)	
				$3/2_1^-$	748	1.6(5)	1.5	100	73		
				$5/2_1^+$	477	n.o.	0.0		0		
				$5/2_1^-$	380	n.o.	0.0		0		

TABLE IV. (*Continued*.)

$E_{x,\mathrm{exp}}$ (keV)	$E_{x,\mathrm{theo}}$ (keV)	τ_{theo} (ps)	J_i^π ($\hbar$)	J_f^π ($\hbar$)	E_γ (keV)	$I_{\gamma,\mathrm{exp}}$ (%)	$I_{\gamma,\mathrm{theo}}$ (%)	b_{exp} (%)	b_{theo} (%)	MBD$_i$	$I_{GT,\mathrm{theo}}$ (%)
1687	1722	0.61	$7/2_1^-$	$9/2_1^+$	1687	13.2(10)	4.9	76(3)	23	0.244(148)	
				$3/2_1^-$	756	n.o.	0.2		1		
				$5/2_1^+$	485	n.o.	0.2		1		
				$5/2_1^-$	388	4.2(5)	16	24(3)	76		
1785	1708	0.28	$13/2_2^+$	$9/2_1^+$	1786	1.5(4)	0.1	26(10)	1	0.191(61)	
				$11/2_1^+$	718	≈4.3	5.7	74(10)	96		
				$13/2_1^+$	550	n.o.	0.2		3		
1841	1879	0.78	$7/2_2^-$	$9/2_1^+$	1841	5.5(7)	5.4	100	39	0.204(108)	
				$3/2_1^-$	910	n.o.	0.8		6		
				$5/2_1^+$	639	n.o.	0.3		2		
				$5/2_1^-$	542	n.o.	6.3		46		
				$7/2_1^-$	154	n.o.	0.4		3		
				$5/2_1^-$	152	n.o.	0.7		5		
1856	1889	1.3	$9/2_1^-$	$9/2_1^+$	1856	15.2(10)	11	93(3)	67	0.095(49)	(0.7)
				$11/2_1^+$	789	n.o.	0.8		5		
				$5/2_1^-$	557	n.o.	0.0		0		
				$7/2_1^-$	169	1.1(5)	4.3	7(3)	27		
1869	1767	13	$17/2_1^-$	$13/2_1^+$	634	n.o.	0.0		0	0.000(79)	
				$15/2_1^-$	257	2.7(6)	0.5	100	100		
1979	2006	1.3	$11/2_1^-$	$9/2_1^+$	1979	15.5(10)	15	71(7)	77	0.034(16)	(1.0)
				$11/2_1^+$	911	1.1(6)	1.6	5(3)	8		
				$13/2_1^+$	744	n.o.	0.8		4		
				$7/2_1^-$	292	n.o.	0.0		0		
				$9/2_1^-$	123	3.6(5)	2.4	24(7)	12		
2018	2079	0.87	$7/2_3^-$	$9/2_1^+$	2018	6.0(7)	7.3	100	57	0.143(67)	
				$3/2_1^-$	1087	n.o.	0.3		2		
				$5/2_1^+$	816	n.o.	0.5		4		
				$5/2_1^-$	719	n.o.	0.6		5		
				$3/2_2^-$	431	n.o.	0.0		0		
				$7/2_1^-$	331	n.o.	0.9		7		
				$(5/2_3^-)$[c]	215	n.o.	3.3		25		
2066	2092	2.9	$13/2_1^-$	$11/2_1^+$	999	n.o.	4.0		23	0.116(43)	(1.5)
				$13/2_1^+$	831	1.6(6)	2.3	31(10)	13		
				$15/2_1^-$	455	3.5(4)	9.8	69(10)	56		
				$11/2_1^-$	87	n.o.	1.4		8		
2175	2170	0.89	$13/2_4^+$	$9/2_1^+$	2175	n.o.	0.0		3	0.089(57)	
				$11/2_1^+$	1108	1.6(4)	0.6	46(14)	70		
				$13/2_1^+$	940	1.9(7)	0.2	54(14)	26		
				$15/2_1^-$	564	n.o.	0.0		1		
2194	2163	0.47	$9/2_2^-$	$9/2_1^+$	2194	1.9(7)	1.5	≈67	40	0.054(27)	(0.0)
				$11/2_1^+$	1127	n.o.	0.2		5		
				$5/2_1^-$	895	n.o.	0.0		1		
				$7/2_1^-$	507	n.o.	0.1		3		
				$7/2_2^-$	352	<2	1.6	≈33	43		
				$9/2_1^-$	338	n.o.	0.2		9		
2195	2215	0.77	$11/2_2^-$	$9/2_1^+$	2195	n.o.	4.5		64	0.156(88)	(0.1)
				$11/2_1^+$	1129	3.9(5)	0.6	43(7)	9		
				$13/2_1^+$	960	n.o.	0.4		5		
				$15/2_1^-$	584	n.o.	0.0		0		
				$7/2_1^-$	508	n.o.	0.0		0		
				$13/2_2^+$	410	n.o.	0.0		0		
				$7/2_2^-$	354	n.o.	0.0		0		
				$9/2_1^-$	339	5.1(8)	1.5	57(7)	21		

TABLE IV. (*Continued*.)

$E_{x,\mathrm{exp}}$ (keV)	$E_{x,\mathrm{theo}}$ (keV)	τ_{theo} (ps)	J_i^π ($\hbar$)	J_f^π ($\hbar$)	E_γ (keV)	$I_{\gamma,\mathrm{exp}}$ (%)	$I_{\gamma,\mathrm{theo}}$ (%)	b_{exp} (%)	b_{theo} (%)	MBD$_i$	$I_{GT,\mathrm{theo}}$ (%)
2219	2224	2.3	$15/2_2^-$	$13/2_1^+$	984	n.o.	0.2		17	0.245(109)	
				$15/2_1^-$	608	n.o.	0.1		8		
				$17/2_1^-$	351	1.8(4)	0.4	100	39		
				$13/2_1^-$	153	n.o.	0.4		35		
2250	2174	0.61	$7/2_4^-$	$9/2_1^+$	2250	1.8(5)	1.6	100	55	0.223(76)	
				$5/2_1^-$	951	n.o.	0.4		14		
				$5/2_2^-$	561	n.o.	0.6		20		
				$(5/2_3^-)$	370	n.o.	0.3		11		
2339	2420	0.73	$11/2_4^-$	$9/2_1^+$	2339	$\approx$7.2	5.8	100	74	0.065(31)	(0.5)
				$11/2_1^+$	1271	n.o.	0.9		12		
				$13/2_1^+$	1103	n.o.	0.6		8		
				$9/2_1^-$	482	n.o.	0.1		1		
				$11/2_1^-$	359	n.o.	0.1		1		
				$13/2_1^-$	272	n.o.	0.1		1		
				$9/2_2^-$	144	n.o.	0.2		2		
				$(9/2_3^-)$	133	n.o.	0.2		2		
2463	2404	0.23	$7/2_6^-$	$9/2_1^+$	2463	4.5(7)	1.6	75(10)	27	0.451(139)	
				$5/2_1^-$	1164	n.o.	3.7		61		
				$7/2_1^-$	777	1.5(6)	0.7	25(10)	11		
(2482)[d]	2618	0.33	$5/2_5^+$	$9/2_1^+$	2482	4.0(10)	0.1	100	1	n/a	5.3
				$3/2_1^-$	1551	n.o.	0.5		10		
				$5/2_1^+$	1280	n.o.	0.7		14		
				$5/2_1^-$	1183	n.o.	0.2		4		
				$7/2_1^+$	819	n.o.	3.8		71		
2586	2631	0.25	$7/2_8^-$	$9/2_1^+$	2586	2.6(6)	0.3	100	34	0.263(102)	
				$5/2_1^-$	1287	n.o.	0.1		11		
				$7/2_1^-$	899	n.o.	0.2		21		
				$9/2_1^-$	730	n.o.	0.2		24		
				$(5/2_3^-)$	706	n.o.	0.1		10		
2676	2841	0.24	$5/2_8^+$	$9/2_1^+$	2676	2.5(5)	2.4	17(4)	11	0.139(53)	22
				$3/2_1^-$	1745	10.3(9)	2.2	72(7)	10		
				$5/2_1^+$	1474	n.o.	7.6		35		
				$5/2_1^-$	1377	n.o.	1.1		5		
				$7/2_1^+$	1013	n.o.	0.0		0		
				$7/2_1^-$	989	n.o.	0.4		2		
				$(7/2_2^+)$	835	n.o.	5.6		26		
				$7/2_3^-$	658	1.5(6)	0.2		1		
				$7/2_3^+$	658	n.o.	2.2		10		
2747	2928	0.60	$1/2_3^+$	$1/2_1^-$	2339	$\approx$16	9.2	83(10)	61	0.087(37)	15
				$3/2_1^-$	1816	1.8(5)	4.4	9(4)	29		
				$5/2_1^+$	1545	n.o.	0.0		0		
				$3/2_2^-$	1160	1.6(5)	1.5	8(4)	8		
				$(3/2_1^+)$	411	n.o.	0.1		1		
				$(1/2_1^+)$	100	n.o.	0.0		0		
2757	2916	0.17	$13/2_7^-$	$9/2_1^+$	2757	n.o.	0.0		0	0.041(12)	13
				$11/2_1^+$	1690	n.o.	0.8		6		
				$13/2_1^+$	1522	n.o.	0.7		5		
				$15/2_1^-$	1146	10.8(10)	11	82(7)	84		
				$11/2_1^-$	779	1.1(5)	0.3	8(4)	2		
				$13/2_1^-$	691	n.o.	0.0		0		
				$15/2_2^-$	582	n.o.	0.1		1		
				$11/2_4^-$	420	1.3(4)	0.1	10(4)	1		

TABLE IV. (*Continued*.)

$E_{x,\mathrm{exp}}$ (keV)	$E_{x,\mathrm{theo}}$ (keV)	τ_{theo} (ps)	J_i^π ($\hbar$)	J_f^π ($\hbar$)	E_γ (keV)	$I_{\gamma,\mathrm{exp}}$ (%)	$I_{\gamma,\mathrm{theo}}$ (%)	b_{exp} (%)	b_{theo} (%)	MBD_i	$I_{GT,\mathrm{theo}}$ (%)
2760	3011	0.31	$9/2^-_{10}$	$9/2^+_1$	2760	3.3(6)	19	21(7)	52	0.096(41)	37
				$7/2^+_1$	1098	6.4(18)	1.1	41(13)	3		
				$7/2^-_1$	1074	5.0(12)	3.4	32(10)	9		
				$7/2^-_2$	919	n.o.	8.2		22		
				$11/2^-_1$	781	n.o.	1.1		3		
				$7/2^-_3$	742	n.o.	1.5		4		
				$7/2^-_4$	509	0.8(5)	0.7	5(4)	2		
				$11/2^-_4$	422	n.o.	0.7		2		
				$7/2^-_6$	297	n.o.	0.4		1		
2765	2985	0.31	$11/2^-_9$	$9/2^+_1$	2765	n.o.	6.9		52	0.261(127)	13
				$11/2^+_1$	1698	n.o.	1.6		12		
				$13/2^+_1$	1530	6.9(7)	1.2		9		
				$15/2^-_1$	1154	n.o.	0.1		1		
				$11/2^-_1$	786	n.o.	2.4		18		
				$(9/2^-_5)$	515	n.o.	0.8		6		
				$11/2^-_4$	427	n.o.	0.4		3		
2825	3005	0.26	$3/2^+_4$	$1/2^-_1$	2417	n.o.	3.6		30	0.231(99)	12
				$3/2^-_1$	1894	n.o.	1.7		14		
				$5/2^+_1$	1623	6.5(7)	3.7	100	31		
				$5/2^-_1$	1526	n.o.	0.8		7		
				$3/2^-_2$	1238	n.o.	0.5		4		
				$(5/2^+_2)$	807	n.o.	1.7		14		
2852	3077	0.17	$13/2^-_{10}$	$9/2^+_1$	2852	n.o.	0.0		0	0.041(10)	30
				$11/2^+_1$	1785	n.o.	2.4		8		
				$13/2^+_1$	1617	n.o.	1.8		6		
				$15/2^-_1$	1241	27.2(20)	25	88(5)	82		
				$11/2^-_1$	873	n.o.	0.6		2		
				$13/2^-_1$	786	n.o.	0.3		1		
				$13/2^+_4$	677	n.o.	0.0		0		
				$11/2^-_2$	658	2.2(7)	0.0		0		
				$15/2^-_2$	634	1.5(6)	0.3		1		
2872	3034	0.42	$9/2^-_{11}$	$9/2^+_1$	2872	1.2(4)	0.0	5(2)	0	0.080(20)	43
				$11/2^+_1$	1805	4.0(6)	8.7	18(5)	20		
				$7/2^-_1$	1185	4.9(5)	3.9	22(6)	9		
				$7/2^-_2$	1031	n.o.	3.9		9		
				$11/2^-_1$	894	1.8(6)	6.5	8(4)	15		
				$7/2^-_3$	854	0.9(5)	6.9	4(3)	16		
				$7/2^-_4$	622	2.5(15)	1.3	11(7)	3		
				$11/2^-_4$	533	1.3(4)	6.1	6(2)	14		
				$7/2^-_6$	409	4.6(6)	5.6	20(6)	13		
				$7/2^-_8$	285	1.4(5)	0.9	6(3)	2		
2894	3027	0.34	$13/2^-_9$	$9/2^+_1$	2894	n.o.	1.7		2	0.091(23)	84
				$11/2^+_1$	1826	3.5(10)	14	9(3)	17		
				$13/2^+_1$	1659	1.0(4)	10	3(1)	12		
				$15/2^-_1$	1282	29.4(16)	29	74(8)	35		
				$11/2^-_1$	915	1.3(6)	5.0	3(2)	6		
				$13/2^-_1$	827	1.7(3)	14	4(1)	17		
				$13/2^+_4$	718	$\approx$3	0.8	8(4)	1		
				$11/2^-_2$	699	n.o.	6.7		8		
				$15/2^-_2$	675	n.o.	0.8		1		

TABLE IV. (*Continued.*)

$E_{x,\mathrm{exp}}$ (keV)	$E_{x,\mathrm{theo}}$ (keV)	τ_{theo} (ps)	J_i^π ($\hbar$)	J_f^π ($\hbar$)	E_γ (keV)	$I_{\gamma,\mathrm{exp}}$ (%)	$I_{\gamma,\mathrm{theo}}$ (%)	b_{exp} (%)	b_{theo} (%)	MBD$_i$	$I_{GT,\mathrm{theo}}$ (%)
2941	3086	0.13	$9/2^-_{12}$	$9/2^+_1$	2941	14.7(10)	5.6	100	26	0.164(78)	21
				$11/2^+_1$	1874	n.o.	1.5		7		
				$7/2^+_1$	1278	n.o.	0.4		2		
				$7/2^-_1$	1254	n.o.	6.5		31		
				$9/2^-_1$	1085	n.o.	1.7		8		
				$7/2^-_3$	923	n.o.	2.7		13		
				$7/2^-_4$	691	n.o.	0.8		4		
				$9/2^-_2$	747	n.o.	0.4		2		
				$(9/2^-_3)$	736	n.o.	1.3		6		
2980[b]	3160	0.13	$5/2^+_{12}$	$9/2^+_1$	2980	n.o.	0.0		1	n/a	3.2
				$3/2^-_1$	2049	n.o.	0.3		9		
				$5/2^+_1$	1778	n.o.	0.5		17		
				$5/2^-_1$	1681	n.o.	0.2		5		
				$7/2^+_1$	1317	n.o.	1.2		38		
				$7/2^-_1$	1293	n.o.	0.1		3		
				$(7/2^+_2)$	1139	n.o.	0.8		25		
2996	3235	0.11	$11/2^-_{14}$	$9/2^+_1$	2996	4.2	2.2	100	28	0.160(80)	7.9
				$11/2^+_1$	1929	n.o.	0.6		6		
				$13/2^+_1$	1761	n.o.	0.5		5		
				$11/2^-_1$	1017	n.o.	3.2		40		
				$13/2^-_1$	930	n.o.	0.3		4		
				$9/2^-_2$	802	n.o.	0.2		3		
				$11/2^-_2$	801	n.o.	0.2		3		
				$9/2^-_3$	791	n.o.	0.3		4		
				$11/2^-_4$	658	n.o.	0.3		4		
3108	3323	0.21	$11/2^-_{15}$	$9/2^+_1$	3108	7.9(12)	5.4	100	50	0.200(78)	11
				$11/2^+_1$	2041	n.o.	1.8		14		
				$13/2^+_1$	1873	n.o.	0.0		0		
				$15/2^-_1$	1497	n.o.	0.0		0		
				$9/2^-_1$	1252	n.o.	1.2		11		
				$11/2^-_1$	1129	n.o.	0.6		6		
				$13/2^-_1$	1042	n.o.	2.0		19		

[a]Not applicable.
[b]Not observed experimentally.
[c]Parentheses indicate a branching into a state which is missing an experimentally observed counterpart.
[d]Parentheses indicate that the decay properties of the predicted and observed state do not match.

[1] M. Arnould, S. Goriely, and K. Takahashi, Phys. Rep. **450**, 97 (2007).
[2] G. Lorusso, S. Nishimura, Z. Y. Xu, A. Jungclaus, Y. Shimizu, G. S. Simpson, P.-A. Söderström, H. Watanabe, F. Browne, P. Doornenbal *et al.*, Phys. Rev. Lett. **114**, 192501 (2015).
[3] M. R. Mumpower, R. Surman, G. C. McLaughlin, and A. Aprahamian, Prog. Part. Nucl. Phys. **86**, 86 (2016).
[4] D. Martin, A. Arcones, W. Nazarewicz, and E. Olsen, Phys. Rev. Lett. **116**, 121101 (2016).
[5] T. Marketin, L. Huther, and G. Martínez-Pinedo, Phys. Rev. C **93**, 025805 (2016).
[6] T. Eronen, V. S. Kolhinen, V.-V. Elomaa, D. Gorelov, U. Hager, J. Hakala, A. Jokinen, A. Kankainen, P. Karvonen, S. Kopecky *et al.*, Eur. Phys. J. A **48**, 46 (2012).
[7] L.-L. Andersson, D. Rudolph, P. Golubev, R.-D. Herzberg, R. Hoischen, E. Merchán, D. Ackermann, Ch. E. Düllmann, K. Eberhardt, J. Even *et al.*, Nucl. Instrum. Methods A **622**, 164 (2010).
[8] P. Hoff, B. Ekström, H. Göktürk, and B. Fogelberg, Nucl. Phys. A **459**, 35 (1986).
[9] D. T. Yordanov, D. L. Balabanski, J. Bieroń, M. L. Bissell, K. Blaum, I. Budinčević, S. Fritzsche, N. Frömmgen, G. Georgiev, Ch. Geppert *et al.*, Phys. Rev. Lett. **110**, 192501 (2013).
[10] D. Lascar, R. Klawitter, C. Babcock, E. Leistenschneider, S. R. Stroberg, B. R. Barquest, A. Finlay, M. Foster, A. T. Gallant, P. Hunt *et al.*, Phys. Rev. C **96**, 044323 (2017).
[11] H. Huck, A. Jech, G. Martí, M. L. Pérez, J. J. Rossi, and H. M. Sofía, Phys. Rev. C **39**, 997 (1989).

[12] D. T. Yordanov, D. L. Balabanski, M. L. Bissell, K. Blaum, I. Budinčević, B. Cheal, K. Flanagan, N. Frömmgen, G. Georgiev, Ch. Geppert *et al.*, Phys. Rev. Lett. **116**, 032501 (2016).

[13] J. Taprogge, A. Jungclaus, H. Grawe, S. Nishimura, P. Doornenbal, G. Lorusso, G. S. Simpson, P.-A. Söderström, T. Sumikama, Z. Y. Xu *et al.*, Phys. Rev. C **91**, 054324 (2015).

[14] O. Arndt, S. Hennrich, N. Hoteling, C. J. Jost, B. E. Tomlin, J. Shergur, K.-L. Kratz, P. F. Mantica, B. A. Brown, R. V. F. Janssens *et al.*, Acta Phys. Pol. B **40**, 437 (2009).

[15] A. Hashizume, Nucl. Data Sheets **112**, 1647 (2011).

[16] H. Gausemel, B. Fogelberg, T. Engeland, M. Hjorth-Jensen, P. Hoff, H. Mach, K. A. Mezilev, and J. P. Omtvedt, Phys. Rev. C **69**, 054307 (2004).

[17] C. Babcock, R. Klawitter, E. Leistenschneider, D. Lascar, B. R. Barquest, A. Finlay, M. Foster, A. T. Gallant, P. Hunt, B. Kootte *et al.*, Phys. Rev. C **97**, 024312 (2018).

[18] M. Hellström, M. N. Mineva, A. Blazhev, H. J. Boardman, J. Ekman, K. Gladnishki, H. Grawe, J. Gerl, R. Page, Z. Podolyák *et al.*, in *Proceedings of the 3rd International Conference on Fission and Properties of the Neutron-Rich Nuclei*, edited by J. Hamilton, A. Ramayya, and H. Carter (World Scientific, Singapore, 2003), p. 22.

[19] A. Scherillo, J. Genevey, J. A. Pinston, A. Covello, H. Faust, A. Gargano, R. Orlandi, G. S. Simpson, I. Tsekhanovich, and N. Warr, Phys. Rev. C **70**, 054318 (2004).

[20] I. D. Moore, T. Eronen, D. Gorelov, J. Hakala, A. Jokinen, A. Kankainen, V. S. Kolhinen, J. Koponen, H. Penttilä, I. Pohjalainen *et al.*, Nucl. Instrum. Methods B **317**, 208 (2013).

[21] P. Karvonen, I. D. Moore, T. Sonoda, T. Kessler, H. Penttilä, K. Peräjärvi, P. Ronkanen, and J. Äystö, Nucl. Instrum. Methods B **266**, 4794 (2008).

[22] A. Nieminen, J. Huikari, A. Jokinen, J. Äystö, P. Campbell, E. C. A. Cochrane (EXOTRAPS Collaboration), Nucl. Instrum. Methods A **469**, 244 (2001).

[23] G. Savard, St. Becker, G. Bollen, H.-J. Kluge, R. B. Moore, Th. Otto, L. Schweikhard, H. Stolzenberg, and U. Wiess, Phys. Lett. A **158**, 247 (1991).

[24] F. Naqvi, M. Górska, L. Cáceres, A. Jungclaus, M. Pfützner, H. Grawe, F. Nowacki, K. Sieja, S. Pietri, E. Werner-Malento *et al.*, Phys. Rev. C **82**, 034323 (2010).

[25] S. Eliseev, K. Blaum, M. Block, C. Droese, M. Goncharov, E. Minaya Ramirez, D. A. Nesterenko, Yu. N. Novikov, and L. Schweikhard, Phys. Rev. Lett. **110**, 082501 (2013).

[26] G. Gräff, H. Kalinowsky, and J. Traut, Z. Phys. A **297**, 35 (1980).

[27] M. König, G. Bollen, H.-J. Kluge, T. Otto, and J. Szerypo, Int. J. Mass Spectrom. **142**, 95 (1995).

[28] J. Eberth, H. G. Thomas, P. v. Brentano, R. M. Lieder, H. M. Jäger, H. Kämmerling, M. Berst, D. Gutknecht, and R. Henck, Nucl. Instrum. Methods A **369**, 135 (1996).

[29] P. M. Jones, L. Wei, F. A. Beck, P. A. Butler, T. Byrski, G. Duchêne, G. de France, F. Hannachi, G. D. Jones, and B. Kharraja *et al.*, Nucl. Instrum. Methods A **362**, 556 (1995).

[30] R. D. Page, A. N. Andreyev, D. E. Appelbe, P. A. Butler, S. J. Freeman, P. T. Greenlees, R.-D. Herzberg, D. G. Jenkins, G. D. Jones, and P. Jones *et al.*, Nucl. Instrum. Methods B **204**, 634 (2003).

[31] P. Golubev, A. Wendt, L. Scruton, J. Taprogge, D. Rudolph, P. Reiter, M. A. Bentley, V. Avdeichikov, P. Boutachkov, and S. P. Fox *et al.*, Nucl. Instrum. Methods A **723**, 55 (2013).

[32] J. Hoffmann *et al.*, GSI Scientific Report 2011, GSI Report 2012-1 (2012).

[33] H. G. Essel and N. Kurz, IEEE Trans. Nucl. Sci. **47**, 337 (2000).

[34] D. C. Radford, Nucl. Instrum. Methods A **361**, 297 (1995).

[35] M. Kretzschmar, Int. J. Mass Spectrom. **264**, 122 (2007).

[36] S. George, K. Blaum, F. Herfurth, A. Herlert, M. Kretzschmar, S. Nagya, S. Schwarz, L. Schweikhard, and C. Yazidjian, Int. J. Mass Spectrom. **264**, 110 (2007).

[37] D. A. Nesterenko, T. Eronen, A. Kankainen, L. Canete, A. Jokinen, I. D. Moore, H. Penttilä, S. Rinta-Antila, A. de Roubin, and M. Vilen, Eur. Phys. J. A **54**, 154 (2018).

[38] Ch. Lorenz, Ph.D. thesis, Lund University, 2019.

[39] M. Tanikawa, H. Kudo, H. Sunaoshi, M. Wada, T. Shinozuka, and M. Fujioka, Z. Phys. A **347**, 53 (1993).

[40] S. Goto, D. Kaji, H. Kudo, M. Fujita, T. Shinozuka, and M. Fujioka, J. Rad. Nucl. Chem. **239**, 109 (1999).

[41] H. Mach, R. L. Gill, D. D. Warner, A. Piotrowski, and R. Moreh, Phys. Rev. C **34**, 1117 (1986).

[42] M. Emeric and A. Sonzogni, LOGFT, NNDC, Brookhaven National Laboratory (2018), https://www.nndc.bnl.gov/logft/

[43] M. Wang, G. Audi, F. G. Kondev, W. J. Huang, S. Naimi, and X. Xu, Chin. Phys. C **41**, 030003 (2017).

[44] S. Ohya, Nucl. Data Sheets **102**, 547 (2004).

[45] J. Katakura, Nucl. Data Sheets **112**, 495 (2011).

[46] J. C. Hardy, L. C. Carraz, B. Jonson, and P. G. Hansen, Phys. Lett. B **71**, 307 (1977).

[47] B. A. Brown and W. D. M. Rae, Nucl. Data Sheets **120**, 115 (2014).

[48] B. A. Brown, Prog. Part. Nucl. Phys. **47**, 517 (2001).

[49] A. Holt, T. Engeland, M. Hjorth-Jensen, and E. Osnes, Nucl. Phys. A **634**, 41 (1998).

[50] L. Coraggio, A. Covello, A. Gargano, N. Itaca, and T. T. S. Kuo, Prog. Part. Nucl. Phys. **62**, 135 (2009).

[51] H. Grawe, K. Langanke, and G. Martínez-Pinedo, Rep. Prog. Phys. **70**, 1525 (2007).

[52] A. Kankainen, J. Hakala, T. Eronen, D. Gorelov, A. Jokinen, V. S. Kolhinen, I. D. Moore, H. Penttilä, S. Rinta-Antila, J. Rissanen, A. Saastamoinen, V. Sonnenschein, and J. Aysto, Phys. Rev. C **87**, 024307 (2013).

[53] J. Taprogge, A. Jungclaus, H. Grawe, S. Nishimura, P. Doornenbal, G. Lorusso, G. S. Simpson, P.-A. Söderström, T. Sumikama, Z. Y. Xu *et al.*, Phys. Rev. Lett. **112**, 132501 (2014); **113**, 049902 (2014).

[54] J. Taprogge, A. Jungclaus, H. Grawe, S. Nishimura, Z. Y. Xu, P. Doornenbal, G. Lorusso, E. Nácher, G. S. Simpson, P.-A. Söderström *et al.*, Phys. Lett. B **738**, 223 (2014).

[55] A. Jungclaus, H. Grawe, S. Nishimura, P. Doornenbal, G. Lorusso, G. S. Simpson, P.-A. Söderström, T. Sumikama, J. Taprogge, Z. Y. Xu *et al.*, Phys. Lett. B **772**, 483 (2017).

[56] E. Caurier, G. Martínez-Pinedo, F. Nowack, A. Poves, and A. P. Zuker, Rev. Mod. Phys. **77**, 427 (2005).

[57] C. B. Hinke, M. Böhmer, P. Boutachkov, T. Faestermann, H. Geissel, J. Gerl, R. Gernhäuser, M. Górska, A. Gottardo, H. Grawe *et al.*, Nature (London) **486**, 341 (2012).

[58] J. Timar, Z. Elekes, and B. Singh, Nucl. Data Sheets **121**, 143 (2014).

[59] M. Hellström *et al.*, GSI Annual Report 2002, GSI report 2003-1, p. 5.

[60] N. Hoteling, W. B. Walters, B. E. Tomlin, P. F. Mantica, J. Pereira, A. Becerril, T. Fleckenstein, A. A. Hecht, G. Lorusso, M. Quinn *et al.*, Phys. Rev. C **76**, 044324 (2007).

[61] D. Kameda, T. Kubo, T. Ohnishi, K. Kusaka, A. Yoshida, K. Yoshida, M. Ohtake, N. Fukuda, H. Takeda, K. Tanaka *et al.*, Phys. Rev. C **86**, 054319 (2012).

[62] M. Rejmund, A. Navin, S. Bhattacharyya, M. Caamaño, E. Clément, O. Delaune, F. Farget, G. de France, B. Jacquot, and A. Lemasson, Phys. Rev. C **93**, 024312 (2016).

[63] D. Rudolph, K. P. Lieb, and H. Grawe, Nucl. Phys. A **597**, 298 (1996).